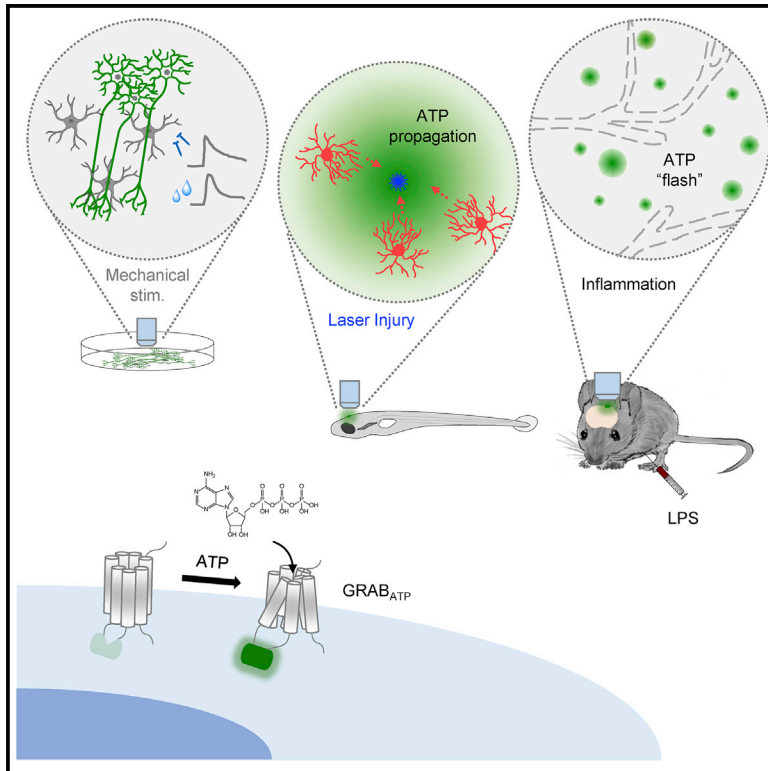# A sensitive GRAB sensor for detecting extracellular ATP *in vitro* and *in vivo*

Graphical abstract

Authors

Zhaofa Wu, Kaikai He, Yue Chen, ..., Jiulin Du, Miao Jing, Yulong Li

Correspondence

wuzhaofa@pku.edu.cn (Z.W.), yulongli@pku.edu.cn (Y.L.)

In brief

Wu et al. developed a sensitive GPCR activation-based ATP sensor, $GRAB_{ATP1.0}$, for monitoring extracellular ATP dynamics under a variety of conditions. In zebrafish, $GRAB_{ATP1.0}$ detected brain injury-induced *in vivo* propagation of ATP. In mouse cortex, $GRAB_{ATP1.0}$ revealed ATP-releasing events at the resolution of a single astrocyte after LPS-induced inflammation.

Highlights

- $GRAB_{ATP}$ is a genetically encoded GPCR activation-based sensor for extracellular ATP

- $GRAB_{ATP}$ can detect ATP with high sensitivity and spatiotemporal resolution

- $GRAB_{ATP}$ reveals injury-induced *in vivo* propagation of ATP in zebrafish larvae

- $GRAB_{ATP}$ reveals LPS-induced local ATP-release events in the mouse cortex *in vivo*

Neuron

CellPress

NeuroResource

A sensitive GRAB sensor for detecting extracellular ATP *in vitro* and *in vivo*

Zhaofa Wu,[1,2,*] Kaikai He,[1,2] Yue Chen,[4] Hongyu Li,[5] Sunlei Pan,[1,2,3] Bohan Li,[1,2] Tingting Liu,[5] Fengxue Xi,[4,6] Fei Deng,[1,2] Huan Wang,[1,2] Jiulin Du,[5] Miao Jing,[4] and Yulong Li[1,2,3,4,7,*]

[1]State Key Laboratory of Membrane Biology, Peking University School of Life Sciences, Beijing 100871, China
[2]PKU-IDG/McGovern Institute for Brain Research, Beijing 100871, China
[3]Peking-Tsinghua Center for Life Sciences, Academy for Advanced Interdisciplinary Studies, Peking University, Beijing 100871, China
[4]Chinese Institute for Brain Research, Beijing 102206, China
[5]Institute of Neuroscience, State Key Laboratory of Neuroscience, Center for Excellence in Brain Science and Intelligence Technology, Chinese Academy of Sciences, 320 Yue-Yang Road, Shanghai 200031, China
[6]School of Basic Medical Sciences, Capital Medical University, Beijing 100069, China
[7]Lead contact
*Correspondence: wuzhaofa@pku.edu.cn (Z.W.), yulongli@pku.edu.cn (Y.L.)
https://doi.org/10.1016/j.neuron.2021.11.027

SUMMARY

The purinergic transmitter ATP (adenosine 5′-triphosphate) plays an essential role in both the central and peripheral nervous systems, and the ability to directly measure extracellular ATP in real time will increase our understanding of its physiological functions. Here, we developed a sensitive GPCR activation-based ATP sensor called GRAB$_{ATP1.0}$, with a robust fluorescence response to extracellular ATP when expressed in several cell types. This sensor has sub-second kinetics, has ATP affinity in the range of tens of nanomolar, and can be used to localize ATP release with subcellular resolution. Using this sensor, we monitored ATP release under a variety of *in vitro* and *in vivo* conditions, including stimuli-induced and spontaneous ATP release in primary hippocampal cultures, injury-induced ATP release in a zebrafish model, and lipopolysaccharides-induced ATP-release events in individual astrocytes in the mouse cortex. Thus, the GRAB$_{ATP1.0}$ sensor is a sensitive, versatile tool for monitoring ATP release and dynamics under both physiological and pathophysiological conditions.

INTRODUCTION

Adenosine 5′-triphosphate (ATP) is a universal energy-storing molecule used by virtually all living organisms. In addition to its metabolic function intracellularly, growing evidence suggests that ATP released into the extracellular space can serve as a signaling molecule (termed purinergic transmitter) (Burnstock, 1972), by binding and activating ionotropic P2X receptors and metabotropic P2Y receptors (Abbracchio et al., 2006; Khakh and North, 2012). In the nervous system, a wide range of functions are regulated by ATP, including pain sensation (Burnstock, 1996; Collier et al., 1966), mechanosensory and chemosensory transduction (Burnstock, 2009; Gourine et al., 2005), and synaptic transmission (Burnstock, 2006). Notably, noxious stimuli in the central nervous system (e.g., injury, low osmolality, inflammation) can trigger a sustained increase in extracellular ATP (Davalos et al., 2005; Wang et al., 2004), which is considered as a multi-target "danger" signal (Rodrigues et al., 2015). Not surprisingly, impaired ATP signaling has been associated with pathological processes (Burnstock, 2007, 2008; Cheffer et al., 2018). Despite the central role ATP plays in both health and disease, the detailed

mechanisms underlying the release and extracellular distribution of ATP are poorly understood, especially *in vivo*.

A significant number of advances in the past few decades have culminated in a variety of techniques and tools for measuring extracellular ATP (Dale, 2021; Wu and Li, 2020). Unfortunately, despite their advantages, these techniques have several key limitations. For example, methods such as microdialysis, electrochemistry-based probes, reporter cells, and bioluminescent assays can measure ATP both *in vitro* and *in vivo* (Pellegatti et al., 2008), but they are severely limited with respect to precisely detecting ATP because of their relatively low spatial and/or temporal resolution. On the other hand, fluorescent sensor-based imaging can provide excellent spatiotemporal resolution (Giepmans et al., 2006), and several fluorescent protein-based sensors have been developed for measuring extracellular ATP, including the recent ecAT3.10 (Conley et al., 2017) and pm-iATPSnFR (Lobas et al., 2019) sensors; however, these sensors are not compatible with measuring extracellular ATP *in vivo*, mainly because of their limited sensitivity and/or signal-to-noise ratio. A recently developed ATP sensor known as ATPOS (ATP optical sensor) has high affinity for ATP and has been used to image extracellular ATP in the mouse cortex (Kitajima et al., 2020);

however, this sensor needs to be injected as a recombinant protein (Kitajima et al., 2020), which may be not easy to penetrate and is difficult to measure ATP in specific cell types. In addition to adapting soluble bacterial F_0F_1-ATP synthase as an ATP-binding protein (e.g., ecAT3.10, pm-iATPSnFR, and ATPOS), the naturally evolved extracellular ATP "detectors"—ATP receptors—were also used to engineer ATP sensors. For example, taking advantage of the permeability to Ca^{2+} ions during ATP-gated P2X channel opening, versatile tools were developed by fusing the genetically encoded Ca^{2+} indicators to the C terminus of P2X subunits (Ollivier et al., 2021; Richler et al., 2008). These sensors display fast kinetics and/or sensitivity allowing the detection of ATP release; however, it might be difficult to exclude that in some conditions, especially under in vivo systems, ATP-P2X-independent activation of GCaMP6s may occur. Overall, the lack of genetically encoded tools that can sense a change in extracellular ATP concentration with high spatiotemporal resolution, high specificity, and high sensitivity has limited our ability to study purinergic signaling under both physiological and pathophysiological conditions.

Recently, our group and others developed a series of genetically encoded G protein-coupled receptor (GPCR) activation-based (GRAB) sensors to measure a variety of neuromodulators—including acetylcholine (Jing et al., 2018, 2020), dopamine (Patriarchi et al., 2018, 2020; Sun et al., 2018, 2020), norepinephrine (Feng et al., 2019), serotonin (Wan et al., 2021), and adenosine (Peng et al., 2020)—with high sensitivity, selectivity, and spatiotemporal resolution, providing the ability to monitor these neuromodulators in targeted cells under in vivo settings. Here, we report the development and application of a new GFP-based GRAB$_{ATP}$ sensor using a P2Y receptor as the ATP-binding scaffold. This sensor, which we call GRAB$_{ATP1.0}$ (or ATP1.0 in brief), can be expressed in a wide range of cell types, producing a robust fluorescence response (with $\Delta F/F_0$ of 500%–1,000%) and with high selectivity for both ATP and ADP; moreover, this sensor can be used to detect changes in extracellular ATP both in vitro and in vivo under a variety of conditions.

RESULTS

Development and characterization of a GRAB sensor for detecting ATP
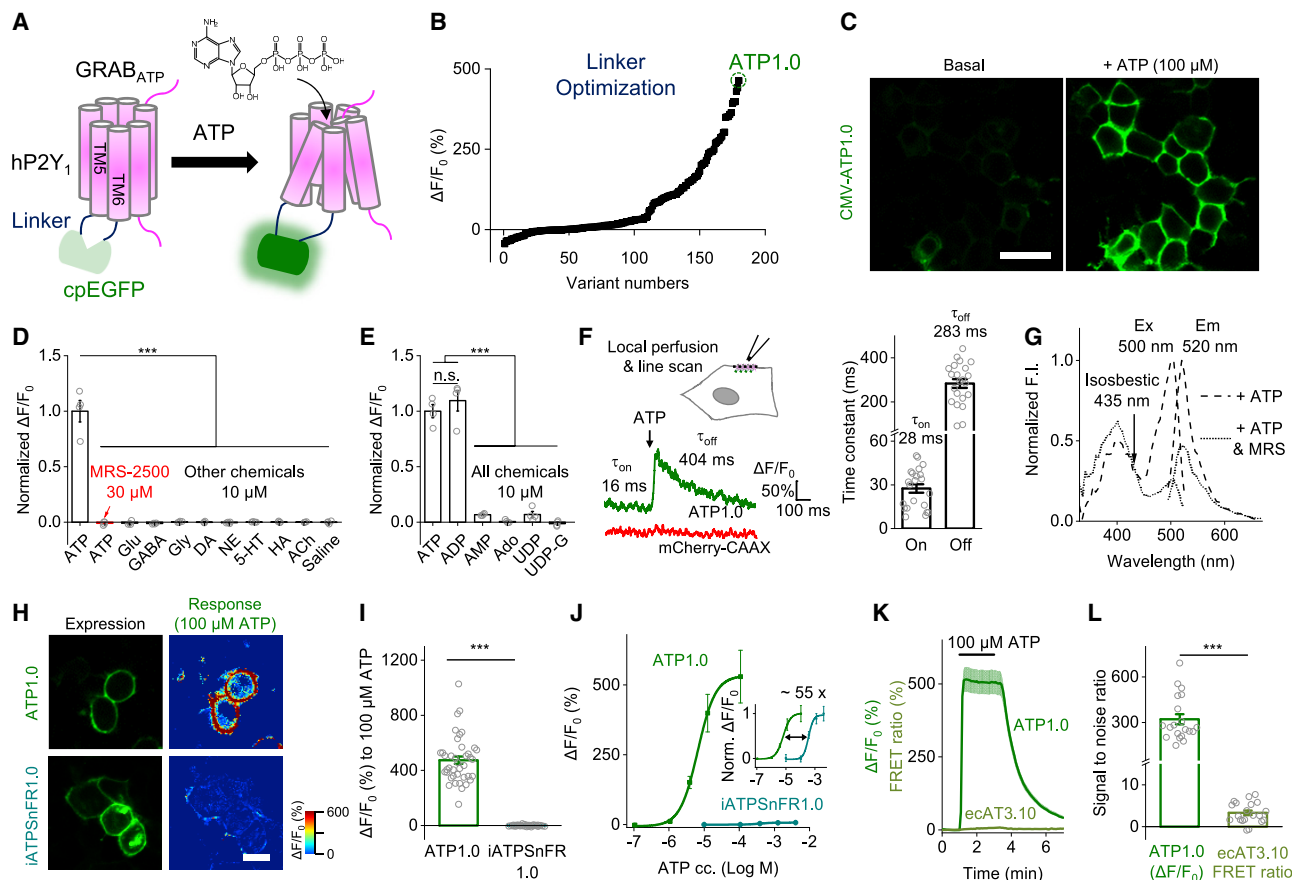
To develop a genetically encoded GRAB sensor for detecting ATP, we first systematically screened a series of candidate G protein-coupled receptors (GPCRs) known to be activated by ATP, including the human P2Y$_1$, P2Y$_2$, P2Y$_4$, P2Y$_{11}$, P2Y$_{12}$, and P2Y$_{13}$ receptors (Xing et al., 2016). Using these GPCRs as the scaffolds, we inserted circularly permuted enhanced GFP (cpEGFP) into the receptor flanked by short linker peptides at both the N and C termini, respectively (Figure S1A); we selected the hP2Y$_1$-based chimera ATP0.1 for further optimization on the basis of its good membrane trafficking and high fluorescence response upon the application of 100 μM ATP (Figure S1B). We then optimized the length and amino acid composition of linkers between the hP2Y$_1$ receptor and the cpEGFP moiety (Figure 1A) and identified the candidate with the largest fluorescence response (Figure 1B); we call this sensor GRAB$_{ATP1.0}$. When ex-

pressed in HEK293T cells, ATP1.0 trafficked to the plasma membrane (Figure 1C) and produced a peak $\Delta F/F_0$ value of ~500% in response to 100 μM extracellular ATP (Figures 1B and 1C). As a negative control, we also generated a mutant version of this sensor called ATP1.0mut, which contains the N283A mutation in the hP2Y$_1$ receptor's ATP-binding pocket (Zhang et al., 2015) and thus is much less sensitive to ATP (Figures S1C and S1D).

We then characterized the specificity, kinetics, brightness, and spectrum of the ATP1.0 sensor. With respect to specificity, the ATP-induced response was fully blocked by the P2Y$_1$ receptor antagonist MRS-2500, and no measurable response was produced by any other neurotransmitters or neuromodulators tested, including glutamate, GABA, glycine, dopamine, norepinephrine, serotonin, histamine, and acetylcholine (Figure 1D). ADP and ATP produced a similar response, whereas structurally similar purinergic molecules or derivatives such as AMP, adenosine, UDP, and UDP-glucose produced virtually no response (Figure 1E). ATP1.0 has rapid response kinetics, with an average rise time constant (τ_{on}) of approximately 28 ms and an average decay time constant (τ_{off}) of approximately 283 ms upon local application of ATP (Figure 1F). With respect to the sensor's brightness, ATP increased the brightness of ATP1.0 to approximately 64% of the brightness measured in cells expressing an hP2Y$_1$-EGFP fusion protein (Figure S1E). Finally, ATP1.0 shows similar spectrum as EGFP under one-photon excitation, with the excitation peak at ~500 nm and emission peak at ~520 nm (Figure 1G).

To compare the performance of ATP1.0 with other extracellular ATP sensors, including a single wavelength-based pm-iATPSnFR sensor (Lobas et al., 2019) and a FRET-based ecAT3.10 sensor (Conley et al., 2017), we expressed these sensors in HEK293T cells and performed confocal imaging. Although ATP1.0 and pm-iATPSnFR1.0 were expressed at similar levels at the plasma membrane (Figure 1H) and have similar brightness (data not shown), cells expressing ATP1.0 had a ~50-fold larger dynamic range to ATP compared with cells expressing pm-iATPSnFR1.0 (Figures 1H–1J). Moreover, compared with cells expressing ATP1.0, cells expressing ecAT3.10 had an extremely small response (Figure 1K) and a significantly smaller signal-to-noise ratio (Figure 1L). We then measured the pH dependency of ATP1.0 used an established experimental system (Jing et al., 2018). Altering extracellular pH with buffers resulted in modest fluorescence changes in ATP1.0-expressing cells (Figure S2A), suggesting a weak extracellular pH dependency of ATP1.0. In a cell membrane permeabilized condition, the fluorescence of ATP1.0 sensors exhibited pH dependency, with a pKa of ~6.7 (Figure S2B). We also measured the dose-dependent responses of ATP1.0 under different temperatures, and ATP1.0-expressing cells show comparable responses and affinity between 25°C and 37°C (Figure S2C).

Next, we examined the performance of ATP1.0 in cultured rat primary astrocytes using an adeno-associated virus (AAV) expressing the sensor under the control of the astrocyte-specific GfaABC1D promoter (Lee et al., 2008). We found that ATP1.0 was widely distributed throughout the plasma membrane, including the soma and cell processes (Figures 2A and S3A). Similarly, when expressed in cultured cortical neurons under

Figure 1. Design, optimization, and characterization of a genetically encoded GRAB$_{ATP}$ sensor

(A) Schematic drawing depicting the principle of GRAB-based ATP sensors designed using the human P2Y$_1$ receptor as the scaffold coupled to the circularly permuted enhanced GFP (cpEGFP). Binding of ATP induces a conformational change that increases the fluorescence signal.

(B) Optimization of the N- and C-terminal linkers connecting the hP2Y$_1$ receptor and the cpEGFP moiety, yielding increasingly responsive ATP sensors. The sensor with the highest response to 100 μM ATP, GRAB$_{ATP1.0}$ (ATP1.0), is indicated.

(C) Representative fluorescence images of HEK293T cells expressing the ATP1.0 sensor under the basal condition and in the presence of 100 μM ATP.

(D and E) Summary of ΔF/F$_0$ measured in ATP1.0-expressing HEK293T cells in the presence of the indicated compounds (each at 10 μM, except for MRS-2500, which was applied at 30 μM), normalized to the peak response measured in ATP; n = 4 independent wells each. ATP, adenosine triphosphate; MRS, MRS-2500; Glu, glutamate; GABA, γ-aminobutyric acid; Gly, glycine; DA, dopamine; NE, norepinephrine; 5-HT, 5-hydroxytryptamine (serotonin); HA, histamine; ACh, acetylcholine; ADP, adenosine diphosphate; AMP, adenosine monophosphate; Ado, adenosine; UDP, uridine diphosphate; UDP-G, UDP-glucose.

(F) Summary of the response kinetics of ATP1.0. Left: the experimental system and representative fluorescence traces of ATP1.0 and co-expressed mCherry-CAAX in HEK293T cell to locally puffed ATP; a line scan was used to measure the fluorescence response, and ATP was puffed with a glass pipette with the duration of ~0.5 s (see STAR Methods for details). Right: the time constant of on and off kinetics of ATP1.0; n = 22 cells from seven coverslips.

(G) Excitation (Ex) and emission (Em) spectra of the ATP1.0 sensor in the presence of ATP (100 μM) or ATP (100 μM) together with MRS-2500 (300 μM). The isosbestic point at 435 nm is indicated.

(H and I) GFP fluorescence images (left column) and pseudocolor images of the response (right column) measured in HEK293T cells expressing ATP1.0 (top row) or pm-iATPSnFR1.0 (bottom row). (I) shows a summary of the response to 100 μM ATP; n = 40 and n = 30 cells each for ATP1.0 and pm-iATPSnFR1.0, respectively.

(J) The peak fluorescence response measured in HEK293T cells expressing ATP1.0 or pm-iATPSnFR1.0 plotted against the indicated concentrations of ATP; n = 10 and n = 20 cells each, respectively. Inset: the same data, normalized and re-plotted.

(K and L) The fluorescence response (K) and signal-to-noise ratio (L) measured in HEK293T cells expressing ATP1.0 or the FRET-based ecAT3.10 sensor; where indicated, 100 μM ATP was applied; n = 20 cells each. The signal-to-noise ratio is defined as the peak response divided by the SD prior to the application of ATP application.

Scale bars represent 30 μm. Summary data are presented as mean ± SEM. The data in (D) and (E) were analyzed using one-way ANOVA followed by Dunnett's post hoc test; the data in (I) and (L) were analyzed using Student's t test; ***p < 0.001; n.s., not significant (p > 0.05). See also Figures S1, S2, and S6.

the control of the neuron-specific human synapsin (hSyn) promotor, ATP1.0 was widely distributed throughout the plasma membrane, including the soma and neurites (Figures 2D and S3B). Both astrocytic and neuronally expressed ATP1.0 responded robustly to ATP application, with averaged peak ΔF/F$_0$ values of approximately 1,000% and 780%, respectively (Figures 2A–2F). Moreover, the ATP-induced fluorescence response was blocked by the P2Y$_1$ receptor antagonist MRS-2500
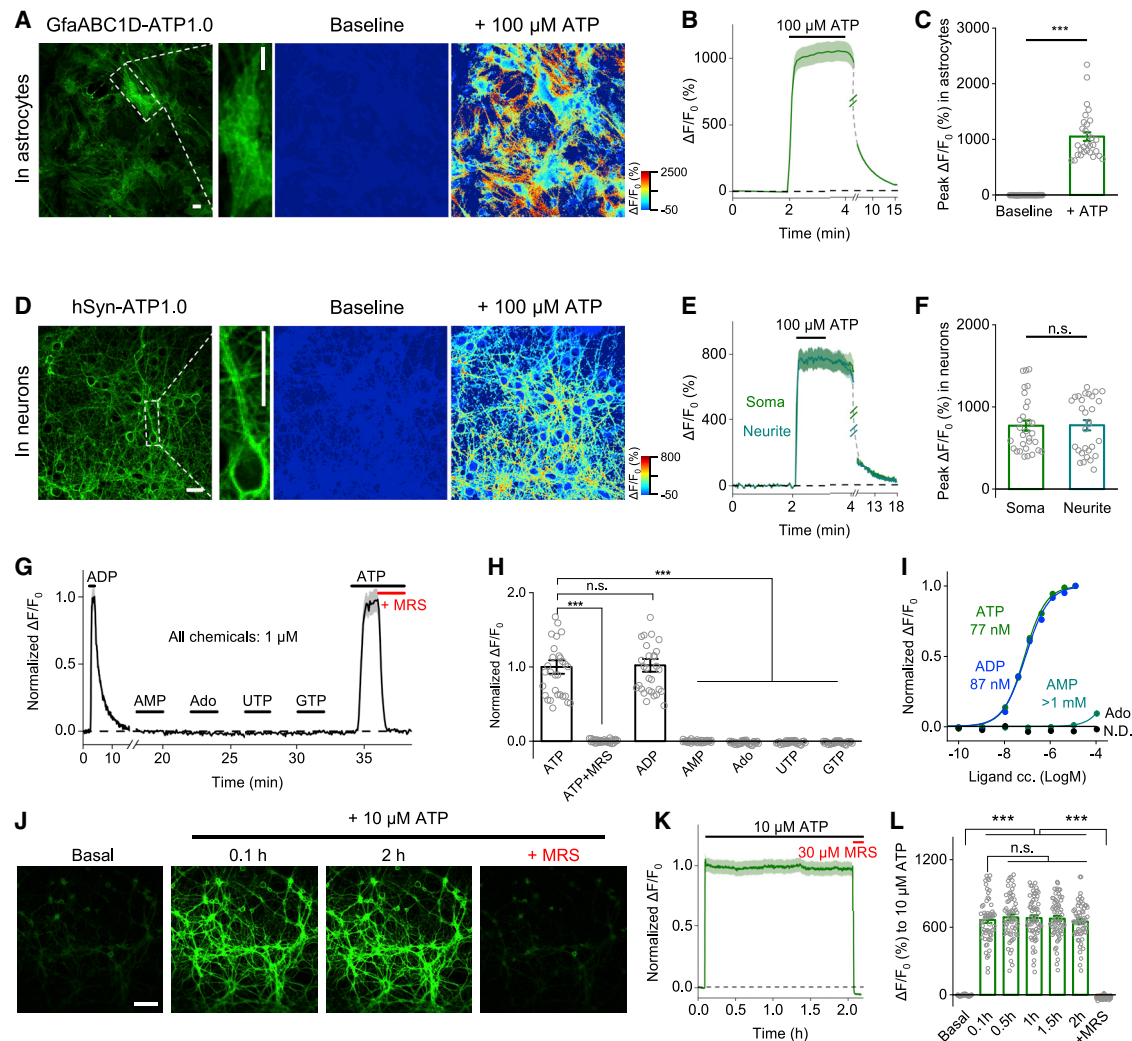
Figure 2. Characterization of the GRAB$_{ATP1.0}$ sensor in primary cultured astrocytes and neurons

(A–C) ATP1.0 was expressed in cultured cortical astrocytes and measured using confocal imaging. (A) Raw GFP fluorescence image (left) and pseudocolor images of the baseline and peak response ($\Delta F/F_0$) to 100 μM ATP. (B) Time course of $\Delta F/F_0$; 100 μM ATP was applied where indicated. (C) Summary of the peak $\Delta F/F_0$ measured before and after application of 100 μM ATP; n = 30 regions of interest (ROIs) each from three coverslips.

(D–F) Same as (A)–(C), except ATP1.0 was expressed in cultured rat cortical neurons; n = 30 ROIs each from three coverslips.

(G–I) Normalized $\Delta F/F_0$ measured in cultured neurons expressing ATP1.0, showing an example trace (G), summary data (H), and dose-response curves with corresponding EC$_{50}$ values (I). UTP, uridine triphosphate; GTP, guanosine triphosphate; N.D., not determined. n = 30–91 ROIs from three coverslips (H and I).

(J–L) Fluorescence image (J), trace (K), and summary (L) of ATP1.0 expressed in cultured hippocampal neurons during a 2 h application of 10 μM ATP; n = 60 neurons from three coverslips.

Scale bars represent 30 μm (A and D) and 100 μm (J). Summary data are presented as mean ± SEM. The data in (C) and (F) were analyzed using Student's t test; the data in (H) and (L) were analyzed using one-way ANOVA followed by Bonferroni's multiple-comparison test; ***p < 0.001; n.s., not significant. See also Figures S3 and S6.

(Figures 2G and 2H), and much lower response was observed in neurons expressing the control ATP1.0mut sensor (Figure S1D). In addition, similar to our results obtained with HEK293T cells, ATP1.0 expressed in neurons responded to both ATP and ADP but did not respond to AMP, adenosine, UTP, or GTP (Figures 2G–2I). Importantly, the ATP1.0 sensor was stable at the cell surface, as we observed no detectable decreases in fluorescence of ATP1.0-expressing neurons during a 2 hours (h) application of 10 μM ATP (Figures 2J–2L).

Taken together, these results indicate that the ATP1.0 sensor is suitable for the use in several cell types, providing a sensitive, specific, and stable fluorescence increase in response to extracellular ATP.

ATP1.0 can be used to monitor the release of ATP from cultures

Next, we examined whether the ATP1.0 sensor could be used to detect the release of endogenous ATP in neuron-glia co-cultures
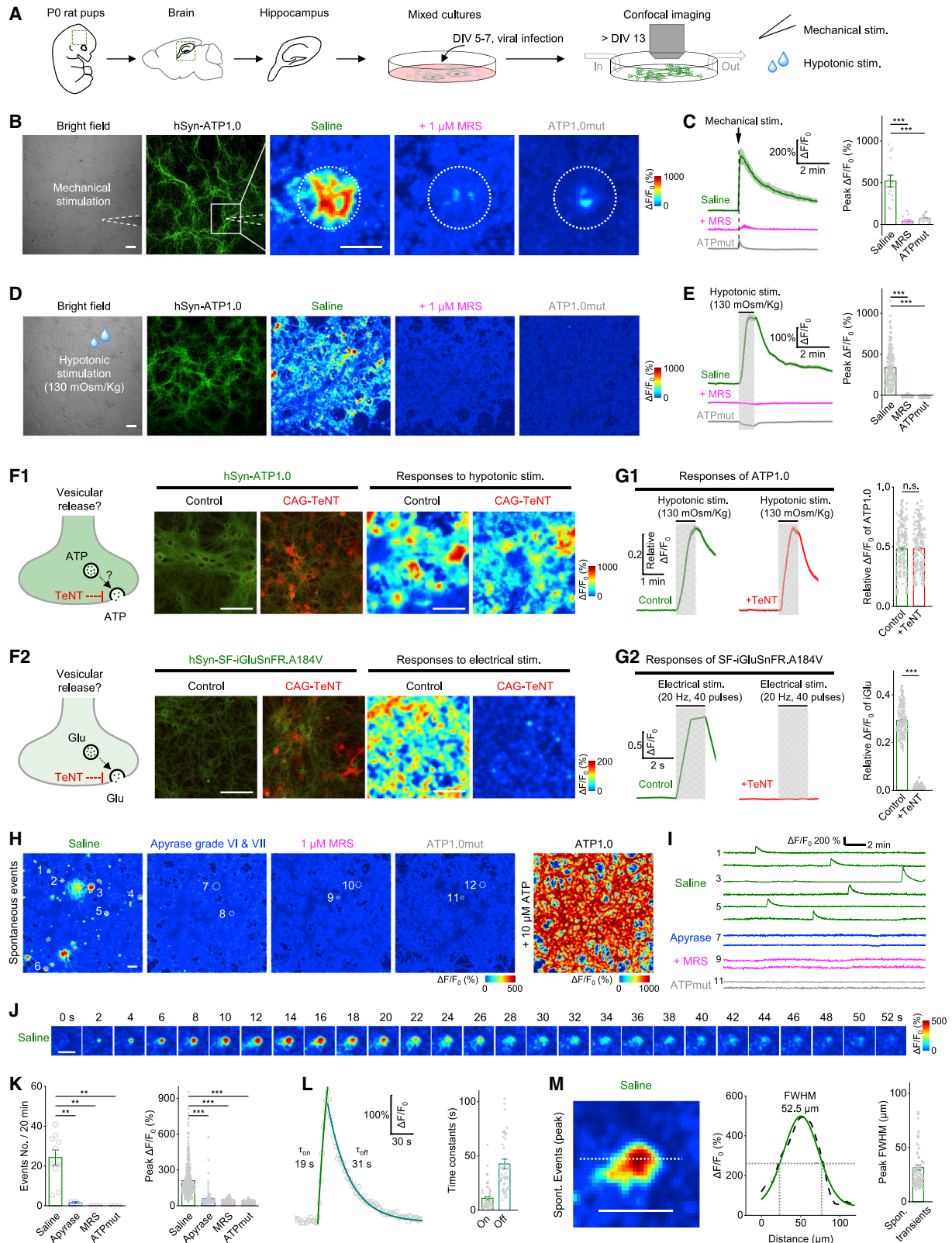
(legend on next page)

(Figure 3A), a widely used system for studying ATP signaling (Fields, 2011; Koizumi et al., 2003; Zhang et al., 2003). Firstly, we tested whether ATP1.0 could detect stimulus-evoked ATP release. In the brain, ATP is released in response to mechanical stimulation and cell swelling (Newman, 2001; Xia et al., 2012). To induce a mechanical stimulus, we pressed a glass pipette against the cultured cells; when the ATP1.0 signal increased, we then removed the pipette to end the stimulus. We found that the mechanical stimulation induced a rapid, localized increase in $\Delta F/F_0$, reflecting the release of ATP (Figure 3B). To induce cell swelling, we bathed the cells in a hypotonic solution (130 mOsm/kg); within 1 min, a robust increase in $\Delta F/F_0$ was observed (Figure 3D). Importantly, the responses induced by both stimuli were abolished by the application of MRS-2500 and were absent in cells expressing the control ATP1.0mut sensor (Figures 3B–3E), confirming the specificity of ATP1.0. We also found that the hypotonic stimulus-induced release of ATP may not require classical SNARE-dependent vesicular releasing machinery, as expressing tetanus toxin light chain (TeNT), which cleaves synaptobrevin and prevents exocytosis (Patterson et al., 2010; Schiavo et al., 1992), had no effect on the response in cells expressing hSyn-ATP1.0 (Figures 3F1 and 3G1); as a control, expressing TeNT abolished the stimulation-evoked release of glutamate (Glu) release measured using the Glu sensor SF-iGluSnFR.A184V (Figures 3F2 and 3G2).

In addition to stimulus-evoked ATP release, we also observed spontaneous, localized and transient ATP1.0 signals in neuron-glia co-cultures even in the absence of external stimulation (Figures 3H and 3I). In the 1.6 mm² imaging field, these events occurred at a rate of 1.2/min and had an average peak $\Delta F/F_0$ of approximately 210% (Figure 3K). The average rise time (τ_{on}) and decay time (τ_{off}) of spontaneous ATP-releasing events were ~11 and ~43 s, respectively (Figure 3L). The average diameter of spontaneous ATP-releasing events was ~32 μm on the basis of our analysis of full width at half maximum (FWHM) (Figure 3M). In contrast, no spontaneous events were observed in the presence of MRS-2500 or in cells expressing ATP1.0mut (Figures

3H, 3I, and 3K). To confirm that the ATP1.0 signal reflects extracellular ATP dynamics, we imaged cells in the presence of the ATP degrading enzyme apyrase. We observed that apyrase (15 U/mL grade VI plus 15 U/mL grade VII) treatment significantly blocked spontaneous events (Figures 3H, 3I, and 3K).

The transient release of ATP was also observed in the previous work using a luciferase-luciferin-based bioluminescent approach under lower extracellular Ca^{2+} conditions. However, the majority of cells exhibited no photodetectable ATP release under basal or normal conditions (Arcuino et al., 2002). They failed to detect ATP release might be because of (1) the relative low sensitivity—the lowest detectable ATP standard was 50 nM as documented—of the bioluminescent approach and/or (2) more time needed to integrate enough photons, which would limit their imaging speed. Taking advantage of the high sensitivity of fluorescent ATP1.0 sensor, we specifically detected ATP release under normal conditions (Figures 3H–3M).

ATP1.0 can be used to measure the injury-induced *in vivo* propagation of ATP in zebrafish larvae

Having shown that the ATP1.0 sensor is suitable for use in *in vitro* systems, we then examined whether it could be applied to monitor ATP dynamics in *in vivo* systems such as in the zebrafish. We therefore transiently expressed either ATP1.0 or ATP1.0mut in neurons of larval zebrafish under the control of the neuron-specific *elavl3* promoter (Figures 4A and 4B). Local puffing of ATP, but not saline, elicited a robust transient increase in $\Delta F/F_0$ in the optic tectum. These signals were blocked by MRS-2500 and not observed in zebrafish larvae expressing the control ATP1.0mut sensor (Figure 4C).

After validating the ATP1.0 sensor could respond to exogenous application of ATP, we then examined whether ATP1.0 could be used to measure the release of endogenous ATP in live zebrafish. Microglia are major immune cells in the brain and respond to brain damage or injury by becoming "activated," a process whereby they rapidly change morphology, proliferate, and migrate to the site of injury (Nimmerjahn et al., 2005; Nolte

Figure 3. GRAB$_{ATP1.0}$ can be used to detect ATP release in primary hippocampal cultures
(A) Schematic diagram depicting the experimental protocol in which primary hippocampal neurons are cultured and infected with an AAV encoding ATP1.0 or ATP1.0mut under the control of the hSyn promoter, followed by confocal fluorescence microscopy during various stimuli. DIV, days *in vitro*.
(B–E) Bright-field images, GFP fluorescence images, pseudocolor images (B and D), and average traces (C and E, left) of the fluorescence response of ATP1.0 or ATP1.0mut measured in saline or 1 μM MRS-2500 (MRS). The white dashed circles in (B) indicate the 150-μm-diameter ROI used for analysis, and the white dashed lines in (B) indicate the location of the electrode used for mechanical stimulation. The summary data (C and E, right) represent 13–20 ROIs from three coverslips (C) and 168–214 ROIs from three or four coverslips (E).
(F1 and G1) Fluorescence images of ATP1.0 (green) and EBFP2-iP2A-TeNT (red) (F1), pseudocolor images (F1), average traces (G1, left), and summary data (G1, right); n = 217–227 ROIs from four coverslips each.
(F2 and G2) Fluorescence images of SF-iGluSnFR.A184V (green) and TeNT-BFP2 (red) (F2), pseudocolor images (F2), average traces (G2, left panels), and summary data (G2, right); n = 171 ROIs from three coverslips each.
(H) Cumulative transient change in ATP1.0 or ATP1.0mut fluorescence measured during 20 min of recording in saline, apyrase (15 U/mL VI plus 15 U/mL VII), or 1 μM MRS-2500. The white dashed circles indicate the ROIs used for the analyses in (I).
(I) Representative traces of $\Delta F/F_0$ measured under the indicated conditions.
(J) Representative time-lapse pseudocolor images captured in saline.
(K) Quantification of the number of events per 20 min (left) and the peak fluorescence response (right) in neurons expressing ATP1.0 or ATP1.0mut; n = 114–363 ROIs from three to ten coverslips.
(L and M) Kinetics profile (L) and spatial profile (M) of the change in ATP1.0 fluorescence measured in saline. The summary in (L) and (M) data represent 54 events and 128 events, respectively, from four coverslips. FWHM, full width at half maximum.
Scale bars represent 100 μm. Summary data are presented as the mean ± SEM. The data in (C) and (E) were analyzed using one-way ANOVA followed by Dunnett's post hoc test; the data in (G) were analyzed using Student's t test; the data in (K) were analyzed using one-way ANOVA followed by Bonferroni's multiple-comparison test. **p < 0.01 and ***p < 0.001; n.s., not significant. See also Figure S7.
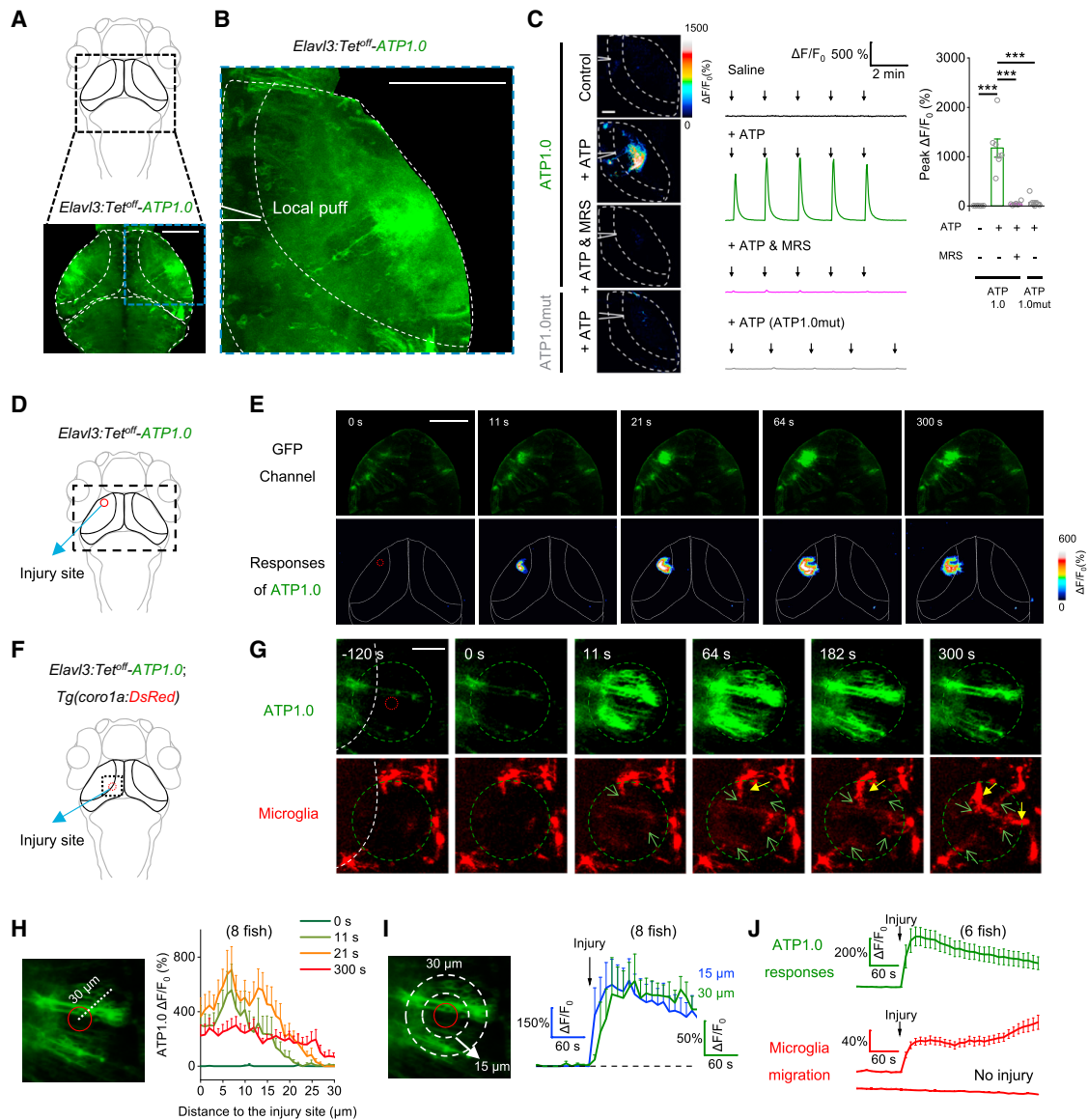
Figure 4. GRAB$_{ATP1.0}$ reveals *in vivo* ATP release induced by injury in a zebrafish model

(A and B) Schematic diagram depicting *in vivo* confocal imaging of fluorescence changes induced by a localized puff (via a micropipette; see inset) of various compounds in the optic tectum of zebrafish larvae expressing ATP1.0 (*Elavl3:Tet^off^-ATP1.0*) or ATP1.0mut (*Elavl3:Tet^off^-ATP1.0mut*).

(C) Representative fluorescence images (left), traces (middle), and summary (right) showing the response of ATP1.0 or ATP1.0mut to the indicated compounds. Arrows indicate the localized application of saline (Control) or ATP (5 mM). Where indicated, MRS-2500 (90 μM) was applied; n = 6 or 7 fishes.

(D) Schematic diagram depicting confocal imaging of ATP1.0 responses before and after two-photon laser ablation (i.e., injury) in the optic tectum of zebrafish larvae expressing ATP1.0. The red dashed circle indicates the region of laser ablation, and the black dashed rectangle indicates the imaging region shown in (E).

(E) Time-lapse pseudocolor images showing the response of ATP1.0 to laser ablation in the optic tectum. The laser ablation was performed at time 0 s and lasted for 7 s, and the ATP1.0 fluorescence was imaged beginning 2 min before laser ablation.

(F) Schematic diagram showing dual-color confocal imaging of ATP release and microglial migration before and after laser ablation in transgenic zebrafish *Tg(coro1a:DsRed)* larvae expressing ATP1.0. In *Tg(coro1a:DsRed)* larvae, the microglia express DsRed. The red dashed circle indicates the region of laser ablation, and the black dashed rectangle indicates imaging region.

(G) *In vivo* time-lapse confocal images showing the migration of microglia (red) and the change in ATP1.0 fluorescence (green) before and after laser ablation (start at time 0 s). The green dashed circle indicates the boundary of the ATP wave at 300 s, and the signal measured in the green dashed circle was used for the analysis in (J). Green arrows indicate the protrusions of microglia entering the green dashed circle; solid yellow arrows indicate the cell bodies of microglia entering the green dashed circle.

(H) Summary of the ATP1.0 response in different distances to the injury site, measured at 0, 11, 21, and 300 s after injury.

(I) Time course of the ATP1.0 response measured at 15 and 30 μm from the site of laser ablation. The arrow shown in traces indicates the beginning of the 7 s laser ablation.

et al., 1996; Thanos and Richter, 1993). It is known that ATP signaling plays key roles in promoting the migration of microglia to injury site not only in mammals (Davalos et al., 2005), but also in fish (Li et al., 2012b; Sieger et al., 2012). In ATP1.0-expressing zebrafish, we found that injury induced by laser ablation in the optic tectum caused a robust increase in fluorescence (Figures 4D and 4E). Moreover, the response propagated in a radial pattern outward from the site of injury (Figures 4E, 4H, and 4I). We analyzed the diameter of released ATP at 11 s and 64 s after injury. The average diameters were ~23 μm and ~34 μm, respectively, on the basis of our analysis of FWHM (Figure S4). Next, we simultaneously monitored ATP release and the migration of microglia by expressing ATP1.0 in the optic tectum of a transgenic zebrafish line in which the microglia are labeled with the red fluorescent protein DsRed (Figure 4F). We found that following laser ablation, microglia gradually migrated to the site of injury along the path of ATP propagation measured using ATP1.0 (Figures 4G and 4J; Video S1). Thus, the ATP1.0 sensor is well suited for *in vivo* application in zebrafish larvae, providing high spatiotemporal resolution.

ATP1.0 can be used to monitor localized ATP release during LPS-induced systemic inflammation in mice

Purinergic signaling molecules, including ATP, are considered as critical extracellular messengers in response to acute and chronic inflammation, acting via paracrine or autocrine processes on immune cells in the peripheral nervous system, as well as on neurons and glia cells in the central nervous system (Idzko et al., 2014). To date, however, the pattern of ATP release during systemic inflammation is poorly understood. We used the intraperitoneal injection of bacterial lipopolysaccharides (LPS) in mice to induce systemic inflammation and directly observed ATP dynamics in the visual cortex using ATP1.0 under a two-photon microscope (Figure 5A). According to previous research, a single dose of LPS (10 mg/kg body weight) (Harland et al., 2020; Hoogland et al., 2015; Maître et al., 2015) was first tested, which induced robust inflammation in the brain with elevated cytokine expression (Figures S5A and S5B). Twenty-four hours after LPS injection, we observed multiple localized ATP-release events in the cortex, with a frequency of approximately 5–10 events/min measured during 20 min of recording (Figures 5B2 and 5D; Video S2). In contrast, fewer events occurred prior to LPS injection (data not shown), in saline-injected controls (Figures 5B1, 5C, and 5E), and no events were observed in LPS-injected mice expressing the control ATP1.0mut sensor (Figures 5B3 and 5C).

Next, we used the Astrocyte Quantitative Analysis (AQuA) software (Wang et al., 2019) to characterize the individual events. The ATP-release events had broadly distributed signal kinetics, although the majority of events have a relatively fast rise time (<5 s) and a slower decay time (10–20 s) (Figures 5F and 5G). In addition, the events had a spatially selective pattern, with an average signal diameter (determined using the maximum

diameter of each event) of approximately 9.9 μm (Figure 5H; Figure S5C1), smaller than the average diameter of a typical astrocyte (10–20 μm) (Chai et al., 2017). The spatial distribution of ATP signals was not determined by the sensor expression level, as the amplitude of fluorescence response did not correlate with basal fluorescence, indicating the spatial selective pattern was not originated from heterogeneous expression of sensor itself (Figures S5C–S5E). These observations are partially in line with previous work, which has documented that the acute injury-induced ATP release is restricted to defined zones (Wang et al., 2004).

To examine in detail the correlation between the ATP-release events and the progression of inflammation, we recorded cortical ATP events at various time points after injection with different dosages of LPS (0.5 and 10 mg/kg, respectively). We found an increase in ATP-release events within 30 min of LPS injection in two doses, and the number of events increased progressively with time, reaching a plateau 2 h and 6 h after 0.5 mg/kg and 10 mg/kg LPS injection, respectively (Figure 5I). In contrast, much fewer events were detected in saline-injected mice at any time point up to 24 h (Figure 5I). Interestingly, an analysis of the location of the ATP-release events within the cortex revealed that the early events occurred relatively close to the blood vessels, and the distance between the events and the nearest vessels increased with time (Figure 5J). These data suggest that the brain can sense inflammation and respond in the form of spatially selective ATP-release events, demonstrating that the ATP1.0 sensor is compatible with *in vivo* imaging in mice, with unprecedented sensitivity and spatiotemporal resolution.

Generation of an ATP sensor with lower affinity and faster kinetics

According to previous studies, the kinetics of GRAB sensors are related to their affinities (Feng et al., 2019; Sun et al., 2018, 2020). For example, the high-affinity dopamine sensor DA1h has slower off kinetics than DA1m (Sun et al., 2018). To generate an ATP sensor with faster kinetics, we further generated a new ATP sensor with lower affinity. After introducing mutations at the DRY motif and ligand binding pockets of hP2Y$_1$-based ATP1.0 (Zhang et al., 2015), we successfully generated a new ATP sensor with lower apparent affinity, namely, ATP1.0-L (Figures S6A and S6B). The off time constant of ATP1.0-L is ~15-fold faster than ATP1.0 upon application of ATP and subsequent application of MRS-2500 (Figure S6C). Moreover, ATP1.0-L slightly increased the fluorescent response toward 100 μM ATP, with half maximal effective concentration (EC$_{50}$) values of ~32 μM and ~56 μM to ATP when expressed in cultured neurons and astrocytes, respectively (Figures S6D and S6E). The hypotonic stimulation induced local ATP1.0-L fluorescence increases in hippocampal neuron-glia co-cultures (Figures S7A–S7E). We also tested the performance of ATP1.0-L in living zebrafish larvae. Similar to the expression of ATP1.0, we transiently

---

(J) Time course of the ATP1.0 response (green) and the microglia migration (red) before and after laser ablation (vertical arrow); also shown is a trace of DsRed fluorescence measured in the area without laser ablation of the same larvae. ROIs 60 μm in diameter are used for analysis.

Scale bars represent 40 μm (B) and (C), 100 μm (E), and 30 μm (G). Data shown in (C) and (J) are presented as mean ± SEM; data shown in (H) and (I) are presented as mean + SEM; numbers in parentheses in (H)–(J) represent the number of zebrafish larvae in each group. The data in (C) were analyzed using Student's t test; ***p < 0.001. See also Figures S4 and S7 and Video S1.
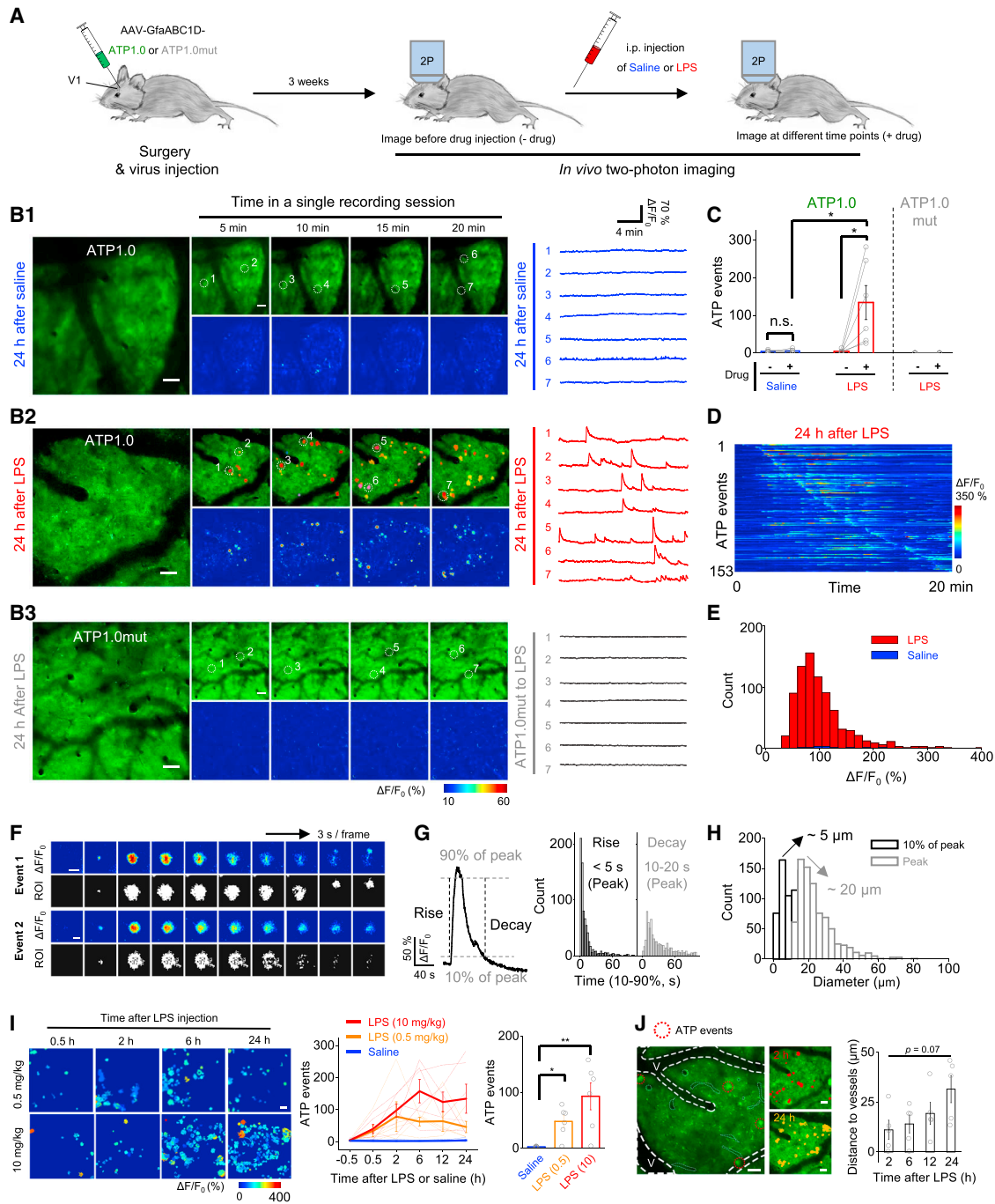
Figure 5. GRAB$_{ATP1.0}$ reveals localized ATP-release events in mouse brain following LPS-induced systemic inflammation

(A) Schematic diagram depicting the experimental protocol in which an AAV encoding either ATP1.0 or ATP1.0mut under the control of the GfaABC1D promoter is injected into the mouse visual cortex (V1), followed by two-photon imaging (2P) through a cranial window at various times after an intraperitoneal (i.p.) injection of saline or lipopolysaccharides (LPS).

(B1 and B2) Representative fluorescence images, pseudocolor images, and individual traces of the fluorescence response of ATP1.0 measured 24 h after saline (B1) or 10 mg/kg LPS (B2) injection. Indicated regions of interest (ROIs, white dashed circles) are identified using AQuA software overlay.

(B3) Same as (B2), except the ATP1.0mut sensor is expressed.

(C) Summary of the number of localized ATP events measured during a 20 min recording before (−) and after (+) saline or 10 mg/kg LPS injection; n = 5 or 6 mice each.

(D) Pseudocolor images showing all the identified ATP events in an exemplar ATP1.0-expressing mice after 24 h LPS injection. The number of identified ATP events from one mouse is shown on the y axis.

(legend continued on next page)

expressed ATP1.0-L in neurons of larval zebrafish under the control of the neuron-specific *elavl3* promoter (Figure S7F). In ATP1.0-L expressing zebrafish, we found that injury induced by laser ablation in the optic tectum also caused increase in fluorescence with faster kinetics, compared with ATP1.0 imaging (Figures S7G–S7I). We hope that the demonstrated use of ATP1.0 and ATP1.0-L during injury of living zebrafish will help elucidate the role of ATP signaling in various disease states.

DISCUSSION

Here, we report the development and characterization of a new, sensitive, genetically encoded ATP sensor called $GRAB_{ATP1.0}$, as well as a low-affinity version, $GRAB_{ATP1.0-L}$. The $GRAB_{ATP1.0}$ sensor enables the high-sensitivity detection of ATP increases in brain tissue, whereas the low-affinity $GRAB_{ATP1.0-L}$ variant could help detect localized ATP release. We show that these sensors can be expressed reliably in a variety of cell types, including cell lines, astrocytes, and neurons, providing robust tools for measuring extracellular ATP. Moreover, we show that these sensors can be used to visualize the real-time release of endogenous ATP *in vitro*, as well as ATP signaling in two *in vivo* models under several conditions.

The $GRAB_{ATP}$ sensors have at least four distinct advantages over other sensors with respect to monitoring the dynamics of extracellular ATP. First, $GRAB_{ATP1.0}$ has extremely high sensitivity for extracellular ATP compared with other ATP sensors such as the recently developed genetically encoded, single-wavelength ATP sensor pm-iATPSnFR1.0. When expressed in HEK293T cells, $GRAB_{ATP1.0}$ displayed an EC_{50} of ~ 6.7 μM, with a maximum $\Delta F/F_0$ of $\sim 500\%$ (Figure 1J). Under the same conditions, pm-iATPSnFR1.0 displayed excellent plasma membrane localization (Figure 1H), yielding an EC_{50} of ~ 381 μM (Figure 1J), which was consistent with published data (Lobas et al., 2019). However, the maximum $\Delta F/F_0$ of pm-iATPSnFR1.0 is $\sim 10\%$, ~ 10-fold lower than reported data (Lobas et al., 2019), presumably because of different imaging conditions. Second, the $GRAB_{ATP}$ sensors are genetically encoded and can be expressed selectively in a variety of cell types, providing cell type-specific measurements of the ATP transmission. Third, the $GRAB_{ATP}$ sensors have high spatial resolution, suitable for measuring highly localized, transient ATP-release events in hip-

pocampal cultures and in the mouse cortex. Last, our results demonstrated that the $GRAB_{ATP}$ sensors can be used to monitor ATP dynamics *in vivo* using a variety of animal models, including zebrafish and mice.

Despite these advantages of genetically encoded $GRAB_{ATP}$ sensors, a potential caveat is that $GRAB_{ATP}$ sensors are based on the scaffold $hP2Y_1$ receptor (Waldo et al., 2002) and therefore respond to both ATP and ADP. Given that ATP and ADP may regulate distinct processes, particularly in the peripheral nervous system (Gaarder et al., 1961), next-generation $GRAB_{ATP}$ sensors should be developed with improved molecular specificity, for example, by engineering the GPCR scaffold to increase the sensor's selectivity for ATP over ADP and vice versa. Alternatively, other P2Y receptors, such as $P2Y_{11}$ and $P2Y_{12}$, which are more specific for ATP (Communi et al., 1997) and ADP (Hollopeter et al., 2001), respectively, can be used as scaffolds in developing future ATP or ADP sensors (Figure S1B). In addition, we found that the $GRAB_{ATP1.0}$ exhibits different apparent affinities to ATP in HEK293T cells (apparent $EC_{50} \sim 6.7$ μM) versus neurons (apparent $EC_{50} \sim 80$ nM). We speculate that one reason is the existence of enzymes that degraded the ATP in cultured HEK293T cells (Uhlen et al., 2017), which reduced the apparent affinities (Figure S2D). Users may need re-calibrate the EC_{50} in their systems.

In hippocampal cultures, the $GRAB_{ATP1.0}$ sensor readily resolved both evoked and spontaneous ATP release. Moreover, our study revealed that the hypotonicity-induced ATP release was not sensitive to TeNT, supporting a non-vesicular mechanism of ATP release (Lazarowski, 2012). Interestingly, several molecules are proposed to mediate stimulus-induced ATP release (Taruno, 2018), including calcium homeostasis modulator (CALHM) (Taruno et al., 2013), pannexin/connexin, P2X7 receptors (Pellegatti et al., 2005), leucine rich repeat containing 8 VRAC subunit A (LRRC8A)/SWELL1 (Qiu et al., 2014; Voss et al., 2014) and SLCO2A1 (Sabirov et al., 2017). We anticipate the new ATP1.0 and ATP1.0-L sensors will provide a good tool to further dissect the relative contributions of these channels on ATP release under different stimulation conditions.

By combining the $GRAB_{ATP1.0}$ sensor with *in vivo* two-photon imaging, we detected highly localized ATP-release events in the mouse brain following a systemic injection of LPS, and we found that these events were smaller in size than the diameter of a single astrocyte (Chai et al., 2017), indicating that the brain can

(E) Distribution of the peak fluorescence response ($\Delta F/F_0$) of the localized ATP events measured in ATP1.0-expressing mice 24 h after 10 mg/kg LPS (red) or saline (blue) injection; n = 805 events from six mice and 25 events from five mice, respectively.

(F) Detailed analysis of the properties of two individual localized ATP events shown as pseudocolor images of $\Delta F/F_0$ and the corresponding ROIs identified using AQuA software at 3 s intervals.

(G) Left: a representative trace (averaged from 50 peak-aligned events) showing the rise and decay kinetics of the event, defined the time between 10% and 90% of the baseline to peak. Right: summary of rise and decay times; n = 805 events from six mice.

(H) Distribution of the size of individual events at 10% of peak response (black) and peak response (gray) measured in ATP1.0-expressing mice 24 h after 10 mg/kg LPS injection; n = 805 events from six mice.

(I) Left: representative images showing ATP-release events (indicated as ROIs) in ATP1.0-expressing mice at the indicated times after 0.5 and 10 mg/kg LPS injection. Middle and right: summary of the number of ATP-release events after 0.5 mg/kg LPS, 10 mg/kg LPS, or saline injection. The data from each individual mouse and the average data are shown. n = 6, n = 6, and n = 5 mice for the 0.5 mg/kg LPS, 10 mg/kg LPS, and saline groups, respectively.

(J) Left: representative image showing early ATP-release events red dashed circles) located near the blood vessel (V, indicated by white dashed lines). Middle, images taken 2 h (red) and 24 h (yellow) after 10 mg/kg LPS injection. Right: summary of the distance between the events and the blood vessel at the indicated times after 10 mg/kg LPS injection; n = 5 mice.

Scale bars represent 50 μm (B, I, and J) and 5 μm (F). Summary data are presented as mean ± SEM. The data in (C) were analyzed using Student's t test; the data in (J) were analyzed using one-way ANOVA followed by Dunnett's post hoc test; $^*p < 0.05$; $^{**}p < 0.01$; n.s., not significant. See also Figure S5 and Video S2.

Neuron
NeuroResource

sense systemic inflammation and respond with ATP signaling at cellular level. Further combining $GRAB_{ATP1.0}$ imaging with genetic and pharmacological tools may facilitate the identification of cell types and molecules required for ATP signaling during these processes. A growing body of experimental evidence suggests that neuroinflammation is a key pathological event triggering and perpetuating the neurodegenerative processes associated with many neurological diseases, including Alzheimer's disease, Parkinson's disease, and amyotrophic lateral sclerosis (Amor et al., 2014; Nguyen et al., 2002). Thus, the $GRAB_{ATP}$ sensors can be powerful tools for studying dynamic changes in ATP release and the role of these changes in the neuroinflammatory processes that underlie neurodegeneration.

ATP plays an important role in neuron-glia interactions, which have complex interactions with other signaling such as calcium or glutamate. For example, the release of ATP can trigger calcium waves in astrocytes and affect neuronal glutamate release (Bazargani and Attwell, 2016; Fields and Burnstock, 2006; Guthrie et al., 1999; Illes et al., 2019; Zhang et al., 2003). Thus, the $GRAB_{ATP}$ sensors can be combined with a spectrally compatible calcium indicator, glutamate sensor, and/or other fluorescent indicators, providing an orthogonal readout of ATP with extremely high spatial and temporal resolution, yielding new insights into the role of ATP signaling under both physiological and pathophysiological processes.

STAR★METHODS

Detailed methods are provided in the online version of this paper and include the following:

- KEY RESOURCES TABLE
- RESOURCE AVAILABILITY
  - Lead contact
  - Materials availability
  - Data and code availability
- EXPERIMENTAL MODEL AND SUBJECT DETAILS
  - Cell lines
  - Primary cell cultures
  - Zebrafish
  - Rats and mice
- METHOD DETAILS
  - Molecular biology
  - AAV virus preparation
  - Expression of $GRAB_{ATP}$ in cultured cells and *in vivo*
  - Confocal imaging of cultured cells
  - *In vivo* confocal imaging of $GRAB_{ATP}$ in larval zebrafish
  - Two-photon *in vivo* imaging in mice
- QUANTIFICATION AND STATISTICAL ANALYSIS

SUPPLEMENTAL INFORMATION

Supplemental information can be found online at https://doi.org/10.1016/j.neuron.2021.11.027.

AUTHOR CONTRIBUTIONS

Y.L. supervised the project. Z.W. and K.H. performed the experiments related to the development, optimization, and characterization of the sensors in cultured cells, with contributions from S.P., B.L., F.X., and H.W. Z.W. performed the imaging of ATP release in cultured cells. H.L. and T.L. performed the *in vivo* zebrafish experiments under the supervision of J.D. Y.C., F.D., and M.J. performed the *in vivo* two-photon imaging experiments in mice. All authors contributed to the interpretation and analysis of the data. Z.W. and Y.L. wrote the manuscript with input from all authors.

DECLARATION OF INTERESTS

Y.L., M.J., and H.W. have filed patent applications (international patent PCT/CN2018/107533), the value of which might be affected by this publication. The remaining authors declare no competing interests.

REFERENCES

Abbracchio, M.P., Burnstock, G., Boeynaems, J.M., Barnard, E.A., Boyer, J.L., Kennedy, C., Knight, G.E., Fumagalli, M., Gachet, C., Jacobson, K.A., and Weisman, G.A. (2006). International Union of Pharmacology LVIII: update on the P2Y G protein-coupled nucleotide receptors: from molecular mechanisms and pathophysiology to therapy. Pharmacol. Rev. *58*, 281–341.

Amor, S., Peferoen, L.A., Vogel, D.Y., Breur, M., van der Valk, P., Baker, D., and van Noort, J.M. (2014). Inflammation in neurodegenerative diseases—an update. Immunology *142*, 151–166.

Arcuino, G., Lin, J.H., Takano, T., Liu, C., Jiang, L., Gao, Q., Kang, J., and Nedergaard, M. (2002). Intercellular calcium signaling mediated by point-source burst release of ATP. Proc. Natl. Acad. Sci. USA *99*, 9840–9845.

Bazargani, N., and Attwell, D. (2016). Astrocyte calcium signaling: the third wave. Nat. Neurosci. *19*, 182–189.

Burnstock, G. (1972). Purinergic nerves. Pharmacol. Rev. *24*, 509–581.

Burnstock, G. (1996). A unifying purinergic hypothesis for the initiation of pain. Lancet *347*, 1604–1605.

Burnstock, G. (2006). Historical review: ATP as a neurotransmitter. Trends Pharmacol. Sci. *27*, 166–176.

Burnstock, G. (2007). Physiology and pathophysiology of purinergic neurotransmission. Physiol. Rev. *87*, 659–797.

Burnstock, G. (2008). Purinergic signalling and disorders of the central nervous system. Nat. Rev. Drug Discov. *7*, 575–590.

Burnstock, G. (2009). Purinergic mechanosensory transduction and visceral pain. Mol. Pain *5*, 69.

Chai, H., Diaz-Castro, B., Shigetomi, E., Monte, E., Octeau, J.C., Yu, X., Cohn, W., Rajendran, P.S., Vondriska, T.M., Whitelegge, J.P., et al. (2017). Neural circuit-specialized astrocytes: transcriptomic, proteomic, morphological, and functional evidence. Neuron *95*, 531–549.e9.

Cheffer, A., Castillo, A.R.G., Corrêa-Velloso, J., Gonçalves, M.C.B., Naaldijk, Y., Nascimento, I.C., Burnstock, G., and Ulrich, H. (2018). Purinergic system in psychiatric diseases. Mol. Psychiatry 23, 94–106.

Collier, H.O., James, G.W., and Schneider, C. (1966). Antagonism by aspirin and fenamates of bronchoconstriction and nociception induced by adenosine-5′-triphosphate. Nature 212, 411–412.

Communi, D., Govaerts, C., Parmentier, M., and Boeynaems, J.M. (1997). Cloning of a human purinergic P2Y receptor coupled to phospholipase C and adenylyl cyclase. J. Biol. Chem. 272, 31969–31973.

Conley, J.M., Radhakrishnan, S., Valentino, S.A., and Tantama, M. (2017). Imaging extracellular ATP with a genetically-encoded, ratiometric fluorescent sensor. PLoS ONE 12, e0187481.

Dale, N. (2021). Biological insights from the direct measurement of purine release. Biochem. Pharmacol. 187, 114416.

Davalos, D., Grutzendler, J., Yang, G., Kim, J.V., Zuo, Y., Jung, S., Littman, D.R., Dustin, M.L., and Gan, W.B. (2005). ATP mediates rapid microglial response to local brain injury in vivo. Nat. Neurosci. 8, 752–758.

Feng, J., Zhang, C., Lischinsky, J.E., Jing, M., Zhou, J., Wang, H., Zhang, Y., Dong, A., Wu, Z., Wu, H., et al. (2019). A genetically encoded fluorescent sensor for rapid and specific in vivo detection of norepinephrine. Neuron 102, 745–761.e8.

Fields, R.D. (2011). Nonsynaptic and nonvesicular ATP release from neurons and relevance to neuron-glia signaling. Semin. Cell Dev. Biol. 22, 214–219.

Fields, R.D., and Burnstock, G. (2006). Purinergic signalling in neuron-glia interactions. Nat. Rev. Neurosci. 7, 423–436.

Gaarder, A., Jonsen, J., Laland, S., Hellem, A., and Owren, P.A. (1961). Adenosine diphosphate in red cells as a factor in the adhesiveness of human blood platelets. Nature 192, 531–532.

Giepmans, B.N., Adams, S.R., Ellisman, M.H., and Tsien, R.Y. (2006). The fluorescent toolbox for assessing protein location and function. Science 312, 217–224.

Gourine, A.V., Llaudet, E., Dale, N., and Spyer, K.M. (2005). ATP is a mediator of chemosensory transduction in the central nervous system. Nature 436, 108–111.

Guthrie, P.B., Knappenberger, J., Segal, M., Bennett, M.V.L., Charles, A.C., and Kater, S.B. (1999). ATP released from astrocytes mediates glial calcium waves. J. Neurosci. 19, 520–528.

Harland, M., Torres, S., Liu, J., and Wang, X. (2020). Neuronal mitochondria modulation of LPS-induced neuroinflammation. J. Neurosci. 40, 1756–1765.

Hollopeter, G., Jantzen, H.M., Vincent, D., Li, G., England, L., Ramakrishnan, V., Yang, R.B., Nurden, P., Nurden, A., Julius, D., and Conley, P.B. (2001). Identification of the platelet ADP receptor targeted by antithrombotic drugs. Nature 409, 202–207.

Hoogland, I.C., Houbolt, C., van Westerloo, D.J., van Gool, W.A., and van de Beek, D. (2015). Systemic inflammation and microglial activation: systematic review of animal experiments. J. Neuroinflammation 12, 114.

Idzko, M., Ferrari, D., and Eltzschig, H.K. (2014). Nucleotide signalling during inflammation. Nature 509, 310–317.

Illes, P., Burnstock, G., and Tang, Y. (2019). Astroglia-derived ATP modulates CNS neuronal circuits. Trends Neurosci. 42, 885–898.

Jing, M., Zhang, P., Wang, G., Feng, J., Mesik, L., Zeng, J., Jiang, H., Wang, S., Looby, J.C., Guagliardo, N.A., et al. (2018). A genetically encoded fluorescent acetylcholine indicator for in vitro and in vivo studies. Nat. Biotechnol. 36, 726–737.

Jing, M., Li, Y., Zeng, J., Huang, P., Skirzewski, M., Kljakic, O., Peng, W., Qian, T., Tan, K., Zou, J., et al. (2020). An optimized acetylcholine sensor for monitoring in vivo cholinergic activity. Nat. Methods 17, 1139–1146.

Khakh, B.S., and North, R.A. (2012). Neuromodulation by extracellular ATP and P2X receptors in the CNS. Neuron 76, 51–69.

Kitajima, N., Takikawa, K., Sekiya, H., Satoh, K., Asanuma, D., Sakamoto, H., Takahashi, S., Hanaoka, K., Urano, Y., Namiki, S., et al. (2020). Real-time in vivo imaging of extracellular ATP in the brain with a hybrid-type fluorescent sensor. eLife 9, e57544.

Koizumi, S., Fujishita, K., Tsuda, M., Shigemoto-Mogami, Y., and Inoue, K. (2003). Dynamic inhibition of excitatory synaptic transmission by astrocyte-derived ATP in hippocampal cultures. Proc. Natl. Acad. Sci. U S A 100, 11023–11028.

Lazarowski, E.R. (2012). Vesicular and conductive mechanisms of nucleotide release. Purinergic Signal. 8, 359–373.

Lee, Y., Messing, A., Su, M., and Brenner, M. (2008). GFAP promoter elements required for region-specific and astrocyte-specific expression. Glia 56, 481–493.

Li, L., Yan, B., Shi, Y.Q., Zhang, W.Q., and Wen, Z.L. (2012a). Live imaging reveals differing roles of macrophages and neutrophils during zebrafish tail fin regeneration. J. Biol. Chem. 287, 25353–25360.

Li, Y., Du, X.F., Liu, C.S., Wen, Z.L., and Du, J.L. (2012b). Reciprocal regulation between resting microglial dynamics and neuronal activity in vivo. Dev. Cell 23, 1189–1202.

Lobas, M.A., Tao, R., Nagai, J., Kronschläger, M.T., Borden, P.M., Marvin, J.S., Looger, L.L., and Khakh, B.S. (2019). A genetically encoded single-wavelength sensor for imaging cytosolic and cell surface ATP. Nat. Commun. 10, 711.

Maître, B., Magnenat, S., Heim, V., Ravanat, C., Evans, R.J., de la Salle, H., Gachet, C., and Hechler, B. (2015). The P2X1 receptor is required for neutrophil extravasation during lipopolysaccharide-induced lethal endotoxemia in mice. J. Immunol. 194, 739–749.

Marvin, J.S., Scholl, B., Wilson, D.E., Podgorski, K., Kazemipour, A., Müller, J.A., Schoch, S., Quiroz, F.J.U., Rebola, N., Bao, H., et al. (2018). Stability, affinity, and chromatic variants of the glutamate sensor iGluSnFR. Nat. Methods 15, 936–939.

Newman, E.A. (2001). Propagation of intercellular calcium waves in retinal astrocytes and Müller cells. J. Neurosci. 21, 2215–2223.

Nguyen, M.D., Julien, J.P., and Rivest, S. (2002). Innate immunity: the missing link in neuroprotection and neurodegeneration? Nat. Rev. Neurosci. 3, 216–227.

Nimmerjahn, A., Kirchhoff, F., and Helmchen, F. (2005). Resting microglial cells are highly dynamic surveillants of brain parenchyma in vivo. Science 308, 1314–1318.

Nolte, C., Möller, T., Walter, T., and Kettenmann, H. (1996). Complement 5a controls motility of murine microglial cells in vitro via activation of an inhibitory G-protein and the rearrangement of the actin cytoskeleton. Neuroscience 73, 1091–1107.

Ollivier, M., Beudez, J., Linck, N., Grutter, T., Compan, V., and Rassendren, F. (2021). P2X-GCaMPs as versatile tools for imaging extracellular ATP signaling. eNeuro 8, ENEURO.0185-20.2020.

Patriarchi, T., Cho, J.R., Merten, K., Howe, M.W., Marley, A., Xiong, W.H., Folk, R.W., Broussard, G.J., Liang, R., Jang, M.J., et al. (2018). Ultrafast neuronal imaging of dopamine dynamics with designed genetically encoded sensors. Science 360, eaat4422.

Patriarchi, T., Mohebi, A., Sun, J., Marley, A., Liang, R., Dong, C., Puhger, K., Mizuno, G.O., Davis, C.M., Wiltgen, B., et al. (2020). An expanded palette of dopamine sensors for multiplex imaging in vivo. Nat. Methods 17, 1147–1155.

Patterson, M.A., Szatmari, E.M., and Yasuda, R. (2010). AMPA receptors are exocytosed in stimulated spines and adjacent dendrites in a Ras-ERK-dependent manner during long-term potentiation. Proc. Natl. Acad. Sci. U S A 107, 15951–15956.

Pellegatti, P., Falzoni, S., Pinton, P., Rizzuto, R., and Di Virgilio, F. (2005). A novel recombinant plasma membrane-targeted luciferase reveals a new pathway for ATP secretion. Mol. Biol. Cell 16, 3659–3665.

Pellegatti, P., Raffaghello, L., Bianchi, G., Piccardi, F., Pistoia, V., and Di Virgilio, F. (2008). Increased level of extracellular ATP at tumor sites: in vivo imaging with plasma membrane luciferase. PLoS ONE 3, e2599.

Neuron
NeuroResource

CellPress

Peng, W., Wu, Z., Song, K., Zhang, S., Li, Y., and Xu, M. (2020). Regulation of sleep homeostasis mediator adenosine by basal forebrain glutamatergic neurons. Science *369*, eabb0556.

Qiu, Z., Dubin, A.E., Mathur, J., Tu, B., Reddy, K., Miraglia, L.J., Reinhardt, J., Orth, A.P., and Patapoutian, A. (2014). SWELL1, a plasma membrane protein, is an essential component of volume-regulated anion channel. Cell *157*, 447–458.

Richler, E., Chaumont, S., Shigetomi, E., Sagasti, A., and Khakh, B.S. (2008). Tracking transmitter-gated P2X cation channel activation in vitro and in vivo. Nat. Methods *5*, 87–93.

Rodrigues, R.J., Tomé, A.R., and Cunha, R.A. (2015). ATP as a multi-target danger signal in the brain. Front. Neurosci. *9*, 148.

Sabirov, R.Z., Merzlyak, P.G., Okada, T., Islam, M.R., Uramoto, H., Mori, T., Makino, Y., Matsuura, H., Xie, Y., and Okada, Y. (2017). The organic anion transporter SLCO2A1 constitutes the core component of the Maxi-Cl channel. EMBO J. *36*, 3309–3324.

Schiavo, G., Benfenati, F., Poulain, B., Rossetto, O., Polverino de Laureto, P., DasGupta, B.R., and Montecucco, C. (1992). Tetanus and botulinum-B neurotoxins block neurotransmitter release by proteolytic cleavage of synaptobrevin. Nature *359*, 832–835.

Schildge, S., Bohrer, C., Beck, K., and Schachtrup, C. (2013). Isolation and culture of mouse cortical astrocytes. J. Vis. Exp. (71), 50079.

Sieger, D., Moritz, C., Ziegenhals, T., Prykhozhij, S., and Peri, F. (2012). Long-range Ca2+ waves transmit brain-damage signals to microglia. Dev. Cell *22*, 1138–1148.

Sun, F., Zeng, J., Jing, M., Zhou, J., Feng, J., Owen, S.F., Luo, Y., Li, F., Wang, H., Yamaguchi, T., et al. (2018). A genetically encoded fluorescent sensor enables rapid and specific detection of dopamine in flies, fish, and mice. Cell *174*, 481–496.e19.

Sun, F., Zhou, J., Dai, B., Qian, T., Zeng, J., Li, X., Zhuo, Y., Zhang, Y., Wang, Y., Qian, C., et al. (2020). Next-generation GRAB sensors for monitoring dopaminergic activity in vivo. Nat. Methods *17*, 1156–1166.

Taruno, A. (2018). ATP release channels. Int. J. Mol. Sci. *19*, 808.

Taruno, A., Vingtdeux, V., Ohmoto, M., Ma, Z., Dvoryanchikov, G., Li, A., Adrien, L., Zhao, H., Leung, S., Abernethy, M., et al. (2013). CALHM1 ion channel mediates purinergic neurotransmission of sweet, bitter and umami tastes. Nature *495*, 223–226.

Thanos, S., and Richter, W. (1993). The migratory potential of vitally labelled microglial cells within the retina of rats with hereditary photoreceptor dystrophy. Int. J. Dev. Neurosci. *11*, 671–680.

Uhlen, M., Zhang, C., Lee, S., Sjöstedt, E., Fagerberg, L., Bidkhori, G., Benfeitas, R., Arif, M., Liu, Z., Edfors, F., et al. (2017). A pathology atlas of the human cancer transcriptome. Science *357*, eaan2507.

Voss, F.K., Ullrich, F., Münch, J., Lazarow, K., Lutter, D., Mah, N., Andrade-Navarro, M.A., von Kries, J.P., Stauber, T., and Jentsch, T.J. (2014). Identification of LRRC8 heteromers as an essential component of the volume-regulated anion channel VRAC. Science *344*, 634–638.

Waldo, G.L., Corbitt, J., Boyer, J.L., Ravi, G., Kim, H.S., Ji, X.D., Lacy, J., Jacobson, K.A., and Harden, T.K. (2002). Quantitation of the P2Y(1) receptor with a high affinity radiolabeled antagonist. Mol. Pharmacol. *62*, 1249–1257.

Wan, J., Peng, W., Li, X., Qian, T., Song, K., Zeng, J., Deng, F., Hao, S., Feng, J., Zhang, P., et al. (2021). A genetically encoded sensor for measuring serotonin dynamics. Nat. Neurosci. *24*, 746–752.

Wang, X., Arcuino, G., Takano, T., Lin, J., Peng, W.G., Wan, P., Li, P., Xu, Q., Liu, Q.S., Goldman, S.A., and Nedergaard, M. (2004). P2X7 receptor inhibition improves recovery after spinal cord injury. Nat. Med. *10*, 821–827.

Wang, Y., DelRosso, N.V., Vaidyanathan, T.V., Cahill, M.K., Reitman, M.E., Pittolo, S., Mi, X., Yu, G., and Poskanzer, K.E. (2019). Accurate quantification of astrocyte and neurotransmitter fluorescence dynamics for single-cell and population-level physiology. Nat. Neurosci. *22*, 1936–1944.

Wu, Z., and Li, Y. (2020). New frontiers in probing the dynamics of purinergic transmitters in vivo. Neurosci. Res. *152*, 35–43.

Wu, J., Abdelfattah, A.S., Zhou, H., Ruangkittisakul, A., Qian, Y., Ballanyi, K., and Campbell, R.E. (2018). Genetically encoded glutamate indicators with altered color and topology. ACS Chem. Biol. *13*, 1832–1837.

Xia, J., Lim, J.C., Lu, W., Beckel, J.M., Macarak, E.J., Laties, A.M., and Mitchell, C.H. (2012). Neurons respond directly to mechanical deformation with pannexin-mediated ATP release and autostimulation of P2X7 receptors. J. Physiol. *590*, 2285–2304.

Xing, S., Grol, M.W., Grutter, P.H., Dixon, S.J., and Komarova, S.V. (2016). Modeling interactions among individual P2 receptors to explain complex response patterns over a wide range of ATP concentrations. Front. Physiol. *7*, 294.

Yu, P.C., Gu, S.Y., Bu, J.W., and Du, J.L. (2010). TRPC1 is essential for in vivo angiogenesis in zebrafish. Circ. Res. *106*, 1221–1232.

Zhang, J.M., Wang, H.K., Ye, C.Q., Ge, W., Chen, Y., Jiang, Z.L., Wu, C.P., Poo, M.M., and Duan, S. (2003). ATP released by astrocytes mediates glutamatergic activity-dependent heterosynaptic suppression. Neuron *40*, 971–982.

Zhang, D., Gao, Z.G., Zhang, K., Kiselev, E., Crane, S., Wang, J., Paoletta, S., Yi, C., Ma, L., Zhang, W., et al. (2015). Two disparate ligand-binding sites in the human P2Y1 receptor. Nature *520*, 317–321.

CellPress

Neuron
NeuroResource

STAR★METHODS

KEY RESOURCES TABLE

REAGENT or RESOURCE	SOURCE	IDENTIFIER
Bacterial and virus strains		
AAV2/9-hSyn-ATP1.0	Vigene Biosciences (this paper)	N/A
AAV2/9-GfaABC1D-ATP1.0	Vigene Biosciences (this paper)	N/A
AAV2/9-hSyn-ATP1.0-L	Vigene Biosciences (this paper)	N/A
AAV2/5-GfaABC1D-ATP1.0-L	Vigene Biosciences (this paper)	N/A
AAV2/9-hSyn-ATP1.0mut	Vigene Biosciences (this paper)	N/A
AAV2/9-GfaABC1D-ATP1.0mut	Vigene Biosciences (this paper)	N/A
AAV2/9-hSyn-SF-iGluSnFR.A184V	Vigene Biosciences (Marvin et al., 2018)	N/A
AAV2/9-hSyn-R^{ncp}-iGluSnFR.	Vigene Biosciences (this paper)	N/A
AAV2/9-CAG-EBFP2-iP2A-TeNT	Vigene Biosciences (this paper)	N/A
Chemicals, peptides, and recombinant proteins		
Disodium ATP	Sigma-Aldrich	CAT#A7699
Disodium ADP	Sigma-Aldrich	CAT#A2754
Disodium AMP	Sigma-Aldrich	CAT#01930
Adenosine (Ado)	Sigma-Aldrich	CAT#A4036
MRS 2500 tetraammonium salt (MRS-2500)	Tocris	CAT#2159
Trisodium GTP	Sigma-Aldrich	CAT#G8877
Trisodium UTP	Santa Cruz	CAT#sc-301964
Disodium UDP	Santa Cruz	CAT#sc-204372
UDP-Glucose	Santa Cruz	CAT#sc-296687
L-Glutamic acid (Glu)	Sigma-Aldrich	Cat#V900408
γ-Aminobutyric acid (GABA)	Tocris	Cat#0344
Glycine (Gly)	Sigma-Aldrich	Cat#G7403
Dopamine hydrochloride (DA)	Sigma-Aldrich	Cat#H8502
Norepinephrine (NE)	Sigma-Aldrich	CAT#A9512
Serotonin hydrochloride (5-HT)	Tocris	Cat#3547
Histamine dihydrochloride (His)	Tocris	Cat#3545
Acetylcholine chloride (ACh)	Solarbio	Cat#G8320
ATPγS	Jena Bioscience	CAT#NU-406
ARL-67156	MREDA	CAT#M063688
PSB-12379	MedChemExpress	CAT#HY-103265B
Apyrase grade VI	Sigma-Aldrich	CAT#A6410
Apyrase grade VII	Sigma-Aldrich	CAT#A6535
2,2,2-Tribromoethanol (Avertin)	Sigma-Aldrich	Cat#T48402
Lipopolysaccharides (LPS)	Sigma-Aldrich	CAT#L4130
Experimental models: Cell lines		
HEK293T	ATCC	Cat#CRL-3216; RRID: CVCL_0063
Experimental models: Organisms/strains		
Rat: Sprague-Dawley rat pups (P0)	Beijing Vital River Laboratory Animal Technology Co., Ltd.	https://www.vitalriver.com/
Mouse: wild-type C57BL/6	Beijing Vital River Laboratory Animal Technology Co., Ltd.	https://www.vitalriver.com/
Zebrafish: Wild-type (AB background)	ZFIN	https://zfin.org/ZDB-GENO-960809-7
Zebrafish: Tg(coro1a:DsRed)	Li et al., 2012a, 2012b	N/A

Neuron
NeuroResource

CellPress

Continued

REAGENT or RESOURCE	SOURCE	IDENTIFIER
Recombinant DNA		
pDisplay-ATP1.0-IRES-mCherry-CAAX	This paper	Addgene: 167582
pDisplay-ATP1.0mut-IRES-mCherry-CAAX	This paper	Addgene: 167583
pDisplay-ATP1.0-L-IRES-mCherry-CAAX	This paper	N/A
pDisplay-hP2Y$_1$-EGFP-IRES-mCherry-CAAX	This paper	N/A
pAAV-hSyn-ATP1.0	This paper	Addgene: 167577
pAAV-hSyn-ATP1.0mut	This paper	Addgene: 167578
pAAV-hSyn-ATP1.0-L	This paper	N/A
pAAV-GfaABC1D-ATP1.0	This paper	Addgene: 167579
pAAV-GfaABC1D-ATP1.0mut	This paper	Addgene: 167580
pAAV-GfaABC1D-ATP1.0-L	This paper	N/A
pm-iATPSnFR1.0	Gift from Dr. Baljit Khakh (Lobas et al., 2019)	Addgene: 102548
ecAT3.10	Gift from Dr. Mathew Tantama (Conley et al., 2017)	Addgene: 107215
Elavl3:Tet^{off}-ATP1.0	This paper	N/A
Elavl3:Tet^{off}-ATP1.0mut	This paper	N/A
Elavl3:Tet^{off}-ATP1.0-L	This paper	N/A
Software and algorithms		
ImageJ	NIH	https://imagej.nih.gov/ij/; RRID: SCR_003070
Origin2019	OriginLab	https://www.originlab.com/; RRID: SCR_014212
GraphPad Prism 5	GraphPad	https://www.graphpad.com/scientific-software/prism/; RRID:SCR_002798
MATLAB	MathWorks	https://www.mathworks.com/products/matlab.html; RRID:SCR_001622
SPSS Statistics 26	IBM Corporation	http://www.spss.com.hk/software/statistics/; RRID:SCR_019096
Astrocyte Quantitative Analysis (AQuA)	Wang et al., 2019	https://github.com/yu-lab-vt/aqua

RESOURCE AVAILABILITY

Lead contact
Further information and requests for resources and reagents should be directed to and will be fulfilled by the lead contact, Yulong Li (yulongli@pku.edu.cn).

Materials availability
The plasmids for expressing ATP1.0 and ATP1.0mut used in this study have been deposited at Addgene (https://www.addgene.org/Yulong_Li/).

Data and code availability
Data and custom programs are available upon request to the lead contact.

EXPERIMENTAL MODEL AND SUBJECT DETAILS

Cell lines
HEK293T cells were obtained from ATCC (CRL-3216) and verified based on their morphology under the microscope and by their growth curve. HEK293T cells were cultured at 37°C in 5% CO_2 in DMEM (Biological Industries) supplemented with 10% (v/v) fetal bovine serum (FBS, GIBCO) and 1% penicillin-streptomycin (Biological Industries).

Primary cell cultures

Primary neuron-glia co-cultures were prepared and cultured as described previously (Peng et al., 2020). In brief, rat primary neuron-glia co-cultures were prepared from 0-day old (P0) rat pups (male and female, randomly selected) purchased from Charles River Laboratories (Beijing, China). Cortical or hippocampal cells were dissociated from the dissected brains in 0.25% Trypsin-EDTA (GIBCO) and plated on 12-mm glass coverslips coated with poly-D-lysine (Sigma-Aldrich) in neurobasal medium (GIBCO) containing 2% B-27 supplement (GIBCO), 1% GlutaMAX (GIBCO), and 1% penicillin-streptomycin (GIBCO). Based on glial cell density, after approximately 4 days in culture (DIV4) cytosine β-D-arabinofuranoside (Sigma) was added to the hippocampal cultures in a 50% growth media exchange, with a final concentration of 2 μM. Primary neuron-glia co-cultures were cultured at 37°C in 5% CO_2.

Rat primary astrocytes were prepared as previously described (Schildge et al., 2013). In brief, the cortex was dissected from P0 rat pups, and the cells were dissociated using trypsin digestion for 10 min at 37°C and plated on a poly-D-lysine–coated T25 flask. The plating and culture media contained DMEM supplemented with 10% (v/v) FBS and 1% penicillin-streptomycin. The next day, and every 2 days thereafter, the medium was changed. At DIV 7-8, the flask was shaken on an orbital shaker at 180 rpm for 30 min, and the supernatant containing the microglia was discarded; 10 mL of fresh astrocyte culture medium was then added to the flask, which was shaken at 240 rpm for $\geq$ 6 h to remove oligodendrocyte precursor cells. The remaining astrocytes were dissociated with trypsin and plated on 12-mm glass coverslips in 24-well plates containing culture medium. Primary astrocytes were cultured at 37°C in 5% CO_2.

Zebrafish

For zebrafish experiments, zebrafish larvae at 4-6 days post-fertilization (4-6 dpf) were used for all experiments in this study. As the sex of zebrafish cannot be determined in the larval stage, sex discrimination was not a factor in our study. Wild-type (AB background) and *Tg(coro1a:DsRed)* (Li et al., 2012a, 2012b) zebrafish lines were used in this study. Adult zebrafish and larvae were maintained and raised under standard laboratory protocols (Yu et al., 2010), and all procedures were approved by the Institute of Neuroscience, Chinese Academy of Sciences.

Rats and mice

All protocols for animal surgery and maintenance were approved by the Animal Care and Use Committees at Peking University and the Chinese Institute for Brain Research, and were performed in accordance with the guidelines established by the US National Institutes of Health. Wild-type Sprague-Dawley rat pups (P0) were used to prepare primary cell cultures. Adult female C57BL/6J mice (6-12 weeks of age) were used for the *in vivo* experiments. Wild-type mice were housed in the animal facility in a temperature-controlled room with a 12 hours-12 hours light-dark cycle with food and water provided *ad libitum*.

METHOD DETAILS

Molecular biology

Plasmids were generated using Gibson assembly. DNA fragments were generated using PCR amplification with primers (Tsingke) with ~25-bp overlap, and all sequences were verified using Sanger sequencing. All cDNAs encoding the candidate GRAB$_{ATP}$ sensors were cloned into the pDisplay vector (Invitrogen) with an upstream IgK leader sequence and a downstream IRES-mCherry-CAAX cassette (to label the cell membrane). The cDNAs encoding the ATP receptor subtypes were amplified from the human GPCR cDNA library (hORFeome database 8.1), and the third intracellular loop (ICL3) of each ATP receptor was swapped with the corresponding ICL3 in the GRAB$_{NE}$ sensor. The swapping sites in the hP2Y$_1$ receptor and the amino acid composition between the hP2Y$_1$ receptor and the ICL3 of GRAB$_{NE}$ were then screened. The plasmids used to express the GRAB$_{ATP}$ sensors in mammalian neurons and astrocytes were cloned into the pAAV vector under the control of human synapsin promoter (hSyn) or the GfaABC1D promoter, respectively. The plasmids used to express the GRAB$_{ATP}$ sensors in zebrafish were cloned into *Elavl3: Tet^{off}* vectors.

The pm-iATPSnFR1.0 sensor was a gift from Baljit Khakh (Addgene plasmid #102548) (Lobas et al., 2019). The ecAT3.10 sensor was a gift from Mathew Tantama (Addgene plasmid #107215) (Conley et al., 2017) . The SF-iGluSnFR.A184V sensor was a gift from Loren Looger (Addgene plasmid #106175) (Marvin et al., 2018). The R^{ncp}-iGluSnFR sensor was a gift from Robert Campbell (Addgene plasmid #107336) (Wu et al., 2018) and was subcloned into the pAAV-hSyn vector. Finally, the plasmid encoding TeNT was a gift from Dr. Peng Cao and was subcloned into the pAAV-CAG vector.

AAV virus preparation

The following AAV viruses were used to infect cultured cells and for *in vivo* expression (all packaged at Vigene Biosciences, China): AAV2/9-hSyn-ATP1.0, AAV2/9-GfaABC1D-ATP1.0, AAV2/9-hSyn-ATP1.0-L, AAV2/5-GfaABC1D-ATP1.0-L, AAV2/9-hSyn-ATP1.0-mut, AAV2/9-GfaABC1D-ATP1.0mut, AAV2/9-CAG-EBFP2-iP2A-TeNT, AAV2/9-hSyn-SF-iGluSnFR.A184V, and AAV2/9-hSyn-R^{ncp}-iGluSnFR.

Expression of GRAB$_{ATP}$ in cultured cells and *in vivo*

For screening, HEK293T cells expressing the candidate GRAB$_{ATP}$ sensors were plated in 96-well plates (PerkinElmer). For confocal imaging, HEK293T cells were plated on 12-mm glass coverslips in 24-well plates and grown to 60%–80% confluence for

Neuron
NeuroResource

CellPress

transfection. Cells were transfected using a mixture containing 1 μg DNA and 1 μg PEI for 4-6 hours and imaged 24-48 hours after transfection. For diffuse *in vitro* expression, the viruses were added to neuron-glia co-cultures or cultured astrocytes at DIV 5-9, and the cells were characterized $\geq$ 48 hours after infection; DIV $\geq$ 13 cells were used for physiological analyses.

For *in vivo* expression in zebrafish, plasmids encoding either ATP1.0, ATP1.0-L or ATP1.0mut were co-injected (25 ng/μl) with *Tol2* transposase mRNA (25 ng/μl) into one-cell stage wild-type (AB background) or *Tg(coro1a:DsRed)* embryos.

To express GRAB$_{ATP}$ in mice *in vivo*, the mice (6-8 weeks) were anesthetized with an i.p. injection of Avertin (500 mg/kg, Sigma); the skin was retracted from the head, and a metal recording chamber was affixed. After the mice recovered for 1-2 days, the mice were re-anesthetized, the cranial window on the visual cortex was opened, and 400-500 nL of AAV was injected using a microsyringe pump (Nanoliter 2000 injector, WPI) at the following coordinates: AP: -2.2 mm relative to Bregma, ML: 2.0 mm relative to Bregma, and DV: 0.5 mm below the dura at an angle of $30°$. A 4 mm x 4 mm square coverslip was used to replace the skull after AAV injection, and *in vivo* two-photon imaging was performed $\sim$3 weeks after injection.

Confocal imaging of cultured cells

Before imaging, the culture medium was replaced with Tyrode's solution contained (in mM): 150 NaCl, 4 KCl, 2 MgCl$_2$, 2 CaCl$_2$, 10 HEPES, and 10 glucose (pH 7.3-7.4). For inducing cell swelling, the hypotonic Tyrode's solution (osmolality: 130 mOsm/kg) contained (in mM): 50 NaCl, 75 KCl, 2 MgCl$_2$, 2 CaCl$_2$, 10 HEPES, and 10 glucose (pH 7.3-7.4). HEK293T cells grown in 96-well plates were imaged using an Opera Phenix high-content screening system (PerkinElmer) equipped with a 20x/0.4 NA objective, a 40x/0.6 NA objective, a 40x/1.15 NA water-immersion objective, a 488-nm laser, and a 561-nm laser; green fluorescence (GRAB$_{ATP}$ sensors and hP2Y$_1$R-EGFP) and red fluorescence (mCherry-CAAX) were recorded using a 525/50-nm and 600/30-nm emission filter, respectively. Cells grown on 12-mm coverslips were imaged using a Ti-E A1 confocal microscope (Nikon) equipped with a 10x/0.45 NA objective, a 20x/0.75 NA objective, a 40x/1.35 NA oil-immersion objective, a 405-nm laser, a 488-nm laser, and a 561-nm laser; blue fluorescence (BFP2-TeNT), green fluorescence (GRAB$_{ATP}$ sensors, iATPSnFR1.0, hP2Y$_1$-EGFP, and SF-iGluSnFR.A184V), and red fluorescence (mCherry-CAAX and R^{ncp}-iGluSnFR) were recorded using a 450/25-nm, 525/50-nm, and 595/50-nm emission filter, respectively. In Figure 1F, the fluorescence changes were imaged by using a Zeiss LSM880 confocal microscope.

The following compounds were applied by replacing the Tyrode's solution (for imaging cells in 96-well plates) or by either bath application or a custom-made perfusion system (for imaging cells cultured on 12-mm coverslips): ATP, ATPγS, ADP, AMP, adenosine, UDP, UTP, GTP, UDP-glucose, MRS-2500, Glu, GABA, Gly, DA, NE, 5-HT, HA, ACh, apyrase grade VI (Sigma A6410) and apyrase grade VII (Sigma A6535), ARL-67156 and PSB-12379. Between experiments, the recording chamber was cleaned thoroughly using Tyrode's solution and 75% ethanol. The micropressure application of drugs was controlled using a Pneumatic PicoPump PV800 (World Precision Instruments). In Figure 1F, ATP was local puffed by using a pulled glass capillary (World Precision Instruments, catalog number: 504949). Glass Capillaries were pulled using the P-97 Micropipette Puller (Sutter Instrument), with following parameters: Heat 580, Pull 35, Vel 50 and Time 150. Hypotonic solutions were delivered by perfusion. For mechanical stimulation, a glass pipette was placed above the cultured cells. For field stimulation of cultured neurons, parallel platinum electrodes positioned $\sim$1-cm apart were controlled using a Grass S88 stimulator (Grass Instruments), and 1-ms pulses were applied at 80 V. Except where indicated, otherwise, all experiments were performed at room temperature.

In vivo confocal imaging of GRAB$_{ATP}$ in larval zebrafish

GRAB$_{ATP}$ responses induced by local puffing of drugs was performed in zebrafish larvae expressing either *Elavl3:Tet^{off}-ATP1.0*, *Elavl3:Tet^{off}-ATP1.0-L* or *Elavl3:Tet^{off}-ATP1.0mut*. GRAB$_{ATP}$ responses and microglia movement following laser ablation–induced injury were performed by using *Tg(coro1a: DsRed)* zebrafish larvae expressing *Elavl3: Tet^{off}-ATP1.0*.

In vivo confocal imaging experiments were performed using an FN1 confocal microscope (Nikon) equipped with a 40x (NA 0.8) or 25 x (NA 1.1) water-immersion objective. Before imaging, the larvae were immobilized in 1.2% low-melting point agarose. Time-series imaging was carried out at 28°C using a heating system. A 488-nm or 561-nm excitation laser and a 525/50-nm or 595/50-nm emission filter were used to excite and collect the GFP and DsRed signals, respectively.

To monitor the GRAB$_{ATP}$ responses to locally puffed drugs, the larvae were paralyzed with 1 mg/ml α-bungarotoxin (Tocris), the agarose around the tectum region were removed, and a small incision in the skin around the top tectum was made for introducing the micropipette. The larvae were incubated in external solution (ES) either with or without 90 μM MRS-2500 (Tocris). Local puff application of ES with or without 5 mM ATP (Sigma) was performed using a micropipette with a tip diameter of 1-2 μm introduced via the contralateral optic tectum to the target tectum region. For each zebrafish larva, the solution contained in the micropipette was puffed using 2 pulses of gas pressure (3 psi, 50-ms duration, 1 s interval), with 5 local puffing sessions in total applied at a 2-min interval. Single optical section confocal imaging was performed with an interval of 2.2 s.

To monitor the GRAB$_{ATP}$ responses and microglial dynamics following laser ablation in larval zebrafish, the larvae were paralyzed and imaged as described above. Time-series images were captured before and immediately after laser ablation. For laser ablation, target regions (5 μm in diameter) were illuminated at 800 nm for 7 s using a two-photon laser.

Two-photon *in vivo* imaging in mice

Two-photon imaging was performed using a FluoView FVMPE-RS microscope (Olympus) equipped a laser (Spectra-Physics). For experiments involving lipopolysaccharides (LPS), 10 mg/kg LPS from *Escherichia coli* O111:B4 (Sigma, L4130) was dissolved in

sterile saline and injected intraperitoneally (i.p.) into the mice. ATP1.0 was imaged using a 920-nm laser, and the imaging frequency was set at 32 Hz with 512x512-pixel resolution.

QUANTIFICATION AND STATISTICAL ANALYSIS

Image data from cultured HEK293T cells, primary cell cultures and larval zebrafish were first processed with ImageJ software (NIH), traces were generated Origin2019 (OriginLab) and pseudocolor images were generated by ImageJ. The signal to noise ratio (SNR) was calculated as the peak response divided by the standard error of the baseline fluorescence fluctuation. Image data from larval zebrafish were first processed with ImageJ, traces were generated by Origin2019 and pseudocolor images were generated by custom-written MATLAB programs. Image data from mice were first processed with Astrocyte Quantitative Analysis (AQuA) (Wang et al., 2019), traces were generated by Origin2019 and pseudocolor images were generated by custom-written MATLAB programs. The fluorescence responses ($\Delta F/F_0$) were calculated as $(F_{raw}-F_{baseline})/F_{baseline}$.

We used Origin2019, GraphPad Prism 5 (GraphPad) and SPSS Statistics 26 (IBM Corporation) to perform the statistical analysis. Sample sizes (n) were reported in figure captions and figure legends. Except where indicated otherwise, groups were analyzed using either the Student's t test or the one-way ANOVA. Except where indicated otherwise, summary data are presented as the mean ± SEM.